Unique and distinct identities and functions of leaf phloem cells revealed by single cell transcriptomics

Short Title: Transcriptome atlas of the Arabidopsis leaf vasculature

Ji-Yun Kim[1,§], Efthymia Symeonidi[2], Tin Yau Pang[3], Tom Denyer[2], Diana Weidauer[1], Margaret Bezrutczyk[1], Manuel Miras [1], Nora Zöllner[1], Michael M. Wudick[1], Martin Lercher[3], Li-Qing Chen[5], Marja C.P Timmermans[2] & Wolf B. Frommer[1,4§]

[1] Institute for Molecular Physiology and Cluster of Excellence on Plant Sciences (CEPLAS), Heinrich-Heine-University Düsseldorf, Düsseldorf 40225, Germany

[2] Center for Plant Molecular Biology, University of Tübingen, Auf der Morgenstelle 32, 72076 Tübingen, Germany

[3] Institute for Computer Science and Department of Biology, Heinrich-Heine-University Düsseldorf, Düsseldorf 40225, Germany

[4] Institute of Transformative Bio-Molecules (WPI-ITbM), Nagoya University, Chikusa, Nagoya 464-8601, Japan

[5] Department of Plant Biology, School of Integrative Biology, University of Illinois at Urbana-Champaign, Urbana, Illinois 61801, U.S.A

ABSTRACT

The leaf vasculature plays a key role in solute translocation. Veins consist of at least seven distinct cell types, with specific roles in transport, metabolism, and signaling. Little is known about the vascular cells in leaves, in particular the phloem parenchyma (PP). PP effluxes sucrose into the apoplasm as a basis for phloem loading; yet PP has only been characterized microscopically. Here, we enriched vascular cells from Arabidopsis leaves to generate a single-cell transcriptome atlas of leaf vasculature. We identified ≥19 cell clusters, encompassing epidermis, guard cells, hydathodes, mesophyll, and all vascular cell types, and used metabolic pathway analysis to define their roles. Clusters comprising PP cells were enriched for transporters, including *SWEET11* and *SWEET12* sucrose and UmamiT amino acid efflux carriers. PP development occurs independently from APL, a transcription factor required for phloem differentiation. PP cells have a unique pattern of amino acid metabolism activity distinct from companion cells (CC), explaining differential distribution/metabolism of amino acids in veins. The kinship relation of the vascular clusters is strikingly similar to the vein morphology, except for a clear separation of CC from the other vascular cells including PP. In summary, our scRNA-seq analysis provides a wide range of information into the leaf vasculature and the role and relationship of the leaf cell types.

KEYWORDS

Arabidopsis, phloem loading, SWEET transporters, sugar transport, amino acid transport, amino acid metabolism, phloem parenchyma, companion cells.

INTRODUCTION

A key feature of multicellularity is the division of labor. During evolution, when plants moved from aquatic to the terrestrial environments, new mechanisms were required for the exchange of nutrients - both photoassimilates from aerial organs to soil-anchored sections, and water and essential nutrients from the soil to the aerial, photosynthetic organs. Terrestrial plants developed complex vascular systems to provide, for example, roots with photoassimilates and to provide a photosynthetic organism with essential nutrients. Cells had to differentiate to acquire unique identities by establishing differential transcriptional networks. The vasculature serves both transport and communication between organs. Arabidopsis leaf veins are conjoint, collateral open and closed bundles, with xylem on the abaxial and phloem on the adaxial side[1]. The veins consist of at least seven different cell types with unique features identifiable by light and electron microscopy. In Arabidopsis, the abaxial phloem is composed of enucleate sieve elements (SE), as the actual conduits, which are coupled to companion cells (CC), and a third, poorly understood cell type, the phloem parenchyma (PP). When mature, the adaxial xylem consists of dead tracheary elements (TE), that are accompanied by xylem parenchyma (XP). The vascular parenchyma (VP) is often located at the interface between phloem and xylem. At earlier stages of development, xylem and phloem are separated by meristematic cells (procambium; open-type vasculature), that differentiate towards the tip of the leaf where procambium is absent (closed-type)[2]. Phloem and xylem exchange water and solutes in complex ways, and thus the cells must be equipped with specific sets of transporters. Moreover, it is likely that the different cell types have specialized metabolic activities. In addition, the vasculature plays important roles in communication by translocating hormones, small RNAs, and even proteins; and also appear to be involved in electrical signaling[3].

PP is one of the poorly defined and least characterized vascular cell types. In Arabidopsis, PP has so-called cell wall ingrowths with a transfer cell appearance that are thought to play a role in amplifying the surface area to allow for higher transport rates[4,5]. Since in many plant species the interface between CC and SE (SE/CC) contains only few plasmodesmata, photoassimilate translocation requires an apoplasmic transport

route[1]. SE/CC loading is mediated by the H^+-sucrose symporter SUT1 (named SUC2 in Arabidopsis), which imports sucrose from the cell wall space[6]. We recently identified sucrose uniporters of the SWEET family in a specific subset of cells in the phloem, that likely represent PP[7]. SWEET expression in PP was confirmed using translational GFP fusions, using a new confocal microscopy method that enabled unambiguous PP identification[8]. A key goal of this work was to characterize the role of PP in more detail by identifying its mRNA outfit. This could serve, for example, as a basis for identifying transporters involved in phloem loading of other nutrients, as well as metabolic pathways active in these cells.

Understanding the complexity of plant cells at a single cell level has long been an active area of interest in plant biology. Comprehension at this level is crucial to determine subtle distinctions between, for example, the multitude of complex vascular cell types. Recently, high throughput single cell RNA-sequencing (scRNA-seq) has been used to provide new insights into root cell biology and development[9–13]. These latest technologies have allowed us to build on the resolution of prior atlases derived from the isolation of specific cell types, using fluorescent activated cell sorting of fluorescently-labelled protoplasts, and/or laser-capture microdissection[14,10,11]. scRNA-seq allows production of comprehensive data with higher resolution and with reduced complications and biases associated with the aforementioned techniques. To gain insights into the specific transcript profiles of the leaf vasculature, we optimized protoplast isolation protocols to enrich for leaf vascular cells. Using scRNA-seq, we identified unique and characteristic mRNA signatures, which revealed fundamental differences in amino acid metabolism and transport pathways in PP and CC important for phloem translocation as well as differences in hormone and glucosinolate metabolism.

RESULTS

Enrichment of vascular protoplasts

Standard protoplast isolation protocols are efficient for protoplasting mesophyll cells for downstream applications such as transient expression. However, these procedures do not efficiently release cells from the vasculature. Here, we developed a methodology for isolating vascular-enriched protoplast populations from mature Arabidopsis leaves (Fig. 1, Supplementary Fig. 1). Initially, a fraction of the non-vascular cell types were removed using the 'tape-sandwich' method which effectively eliminated trichomes, guard cells, and epidermis from the abaxial leaf surface (Supplementary Fig. 1b)[15]. Cuts along the midvein further facilitated access of cell wall digesting enzymes to the vasculature (Fig. 1a, Supplementary Fig. 1b). Elevated concentrations of mannitol lead to an increased release of protoplasts (Fig. 1b, Supplementary Fig. 1c,d). We monitored the release by light microscopy, RT-qPCR, and fluorescence microscopy. The mRNA levels of marker genes were used to evaluate the enrichment of vascular protoplasts during optimization of the protocols (Fig. 1a-c). In addition, the release of intact vascular protoplasts was verified microscopically by monitoring fluorescently-labeled cells using stably transformed Arabidopsis lines expressing *pAtSWEET11:AtSWEET11-GFP*, a tentative marker for PP[7], and *Q0990*, a procambial marker[16] (Fig. 1d,e, Supplementary Fig. 1e. The bulk leaf (not subjected to protoplasting) transcriptome showed high correlation with bulk protoplast transcriptomes (Pearson´s correlation coefficient of 0.9) (Supplementary Fig. 2a, Supplementary Table 1). The high correlation indicates that the protoplasting protocol used here did not impact the relative abundance of cells in the leaf and supported the notion that the scRNA-seq data derived from the protoplasts should cover essentially all cell types present in a mature leaf (the term enriched here thus refers to enrichment over standard protocols).

Single cell RNA-sequencing of vascular-enriched leaf protoplast population

scRNA-seq libraries were produced from vasculature-enriched leaf protoplast populations, with 5,230 single-cell transcriptomes obtained from two biological replicates. Sequencing to a depth of ~96,000 reads per cell was undertaken, and identified a median number of 3,342 genes, and 27,159 unique molecular identifiers

(UMIs, representing unique transcripts), per cell (Supplementary Fig. 2b). Unsupervised clustering using Seurat[17] identified 19 distinct cell clusters (Fig. 2a, Supplementary Video 1, Supplementary Table 2). Plotting the transcriptomes from the two replicates in two dimensions using Uniform Manifold Approximation and Projection (UMAP)[18] revealed an overlapping distributions of cells, and a similar proportion of cell identities (Supplementary Fig. 2c). mRNA profiles and relative cell numbers in the clusters were highly correlated in the replicates (Supplementary Table 2). To assign cell identity to the clusters, we examined the specificity of transcripts of known marker genes (Fig. 3, Supplementary Fig. 3, Supplementary Table 3 and 4).

The 19 clusters cover all major cell types of the leaf. The population was dominated by mesophyll cells (~75% of all cells). as indicated by the enrichment of known mesophyll markers (*CAB3*, *LHCB2.1*, and *CA1*)[19,20] (Fig. 3, Supplementary Fig. 3a). The mesophyll group comprised twelve clusters (Clusters, or C1, 2, 3, 5, 6-9, 11, 12, 14; Fig. 2a, Fig. 3; Supplementary Table 4) and formed three major branches on the UMAP plot. Naively, two separate mesophyll clusters can be expected, one for palisade and one for spongy parenchyma. *FIL* (*YAB1*) transcripts, markers for spongy parenchyma were enriched in C2 and C7, possibly indicating that these clusters may represent spongy parenchyma (Supplementary Fig. 3a)[21]. Among the mesophyll clusters, C6 and C9 were enriched for rRNAs (Supplementary Table 4). We did not remove rRNA before sample preparation and did not filter cells that showed higher rRNA transcript levels since rRNA levels can vary between cells. Whether C6 and 9 represent unique biologically relevant cell populations in the leaf or are due to artifacts was not further evaluated. While the mesophyll clusters likely contain interesting information, we did not characterize them further, as we decided to focus on the vasculature.

Beyond the mesophyll, epidermal cells were identified in C13, based on enrichment of the epidermis-specific transcription factor *AtML1*[22] and wax-related genes (Fig. 3). Epidermal guard cells were found in C16, indicated by the specific enrichment of *FAMA* and guard cell-specific MAP kinases (Fig. 3, Supplementary Fig. 3a). Enrichment of transcripts of the purine transporter *PUP1* and the homolog of carrot chitinase, *EP3*, indicated that C17 comprises hydathodes cells (Supplementary Fig. 3a)[23].

Several clusters showed a vasculature identity, based on the enrichment of known marker genes, indicating that the enrichment for these cell types was successful. The vasculature is composed of phloem and xylem, often separated by a meristematic layer, the procambium, which initiates and maintains vascular organization. We assigned clusters to the seven known cell types present in leaves (Fig. 2). Additionally, we identified cell types with identities that had properties of two cell types, e.g. xylem and procambium.

Cluster 4 was found to contain bundle sheath (BS) and xylem cells and was subsequently subclustered into three cell populations, C4.1, C4.2, and C4.3 (Fig. 2b, Supplementary Table 5). Subclusters C4.2 and C4.3 were enriched for the BS marker *SCL23,* and the sulfate transporter, *SULTR2;2* (Fig. 2b, Fig. 3, Supplementary Fig. 3b,c). C4.2 was enriched for genes involved in photosynthetic processes, possibly indicating a differentiation of BS cells (Supplementary Table 5). The existence of two BS clusters is consistent with morphological descriptions[24]. C4.1, C10, C15, and C18, with a total of 478 cells, were assigned as vascular cell types (Fig. 2, Fig. 3, Supplementary Fig. 3a, Supplementary Table 3).

Degree of kinship relations among BS, XP, PC and PP

Clusters composed of BS, xylem parenchyma (XP) and procambial (PC), and PP cells show a J-shaped relatedness in our UMAP plot (Fig. 2). BS is related to two types of xylem cells (XP1 and XP2), that abut the PC. PC subclusters into two subsets closely related to XP1 (PC^{XP}) and PP1 (PC^{PP}), respectively. The PC^{PP} is adjacent to the two PP clusters PP1 and PP2. XP3 and PP2 form a separate group, which together with XP2, form the hook of the J shape in our UMAP plot (Fig. 2b).

Xylem-related clusters

The enrichment of *GLR3;6*[3] and *ACL5* markers identified C4.1 as parenchymatic xylem cells (Supplementary Fig. 3a,d-i). Further clustering of C4.1 resulted in two subgroups, XP1 and XP2, distinguished by the relative enrichment of photosynthetic genes (Supplementary Table 5). An additional subcluster with xylem identity, XP3, was observed as a subgroup of cells from C18. XP3 was enriched with xylem markers as well as those for vascular parenchyma[25] (Supplementary Fig. 3d-i, Supplementary Fig. 4). Transport proteins were enriched in the xylem clusters (XP1-XP3), as one may expect from their role in supplying tracheal elements

with ions and nutrients for xylem translocation. These included amino acid transporters, such as the H^+/amino acid symporter *AAP6* and the UmamiT amino acid exporter family member *UmamiT22* (refs.[26–28]). The amino acid export protein *GDU4* was also enriched in the xylem clusters. Multiple SULTR low-affinity sulfate transporters, which play pivotal roles in sulfate transport in xylem parenchyma cells, were detected in the xylem cells as well as the boron transporter *NIP6.1*, the glucosinolate importer *GTR2/NPF2.11*[29,30], the heavy metal transporter *HMA2*, and the plastidic bile acid transporter *BAT5*/*BASS5* (Supplementary Table 6).

Phloem- and xylem-related subpopulations of the procambial subclusters

Arabidopsis procambium constitutes a bifacial stem cell population producing xylem on the adaxial pole and phloem on the abaxial pole[32,33]. On our UMAP plot, the XP clusters are in proximity to Cluster 10. Cluster 10 could be further subdivided into three subclusters: the PP1 (C10.2) and two distinct procambial populations, C10.1.1 and C10.1.2 (Fig. 2, Fig. 4a, Supplementary Tables 7 and 8). While cells in PC^{PP} corresponds to procambial cells involved in the maintenance of meristematic identity and the differentiation of phloem cells, cells of PC^{XP} appear to be more closely related to the formation of xylem cells, and is located closer to the XP clusters (Fig. 4, Supplementary Tables 7 and 8).

Cells in the PC^{XP} cluster were enriched with transcripts for homeodomain leucine-zipper (HD-Zip) transcription factor, *HOMEOBOX GENE 8* (*HB-8*)[33] transcripts, known to trigger xylem differentiation (Fig. 4b). Adaxial HD-Zip transcription factors, such as *REVOLUTA/INTERFASCICULAR FIBERLESS1* (*REV/IFL1*), *PHABULOSA* (*PHB*), and *CORONA* (*CNA/AtHB15*), were also enriched in this cluster (Fig. 4c,d, Supplementary Fig. 5). Conversely, the PC^{PP} cluster closest to the PC^{XP} was enriched with known factors involved in the maintenance of protophloem identity and pluripotency, such as *COTYLEDON VASCULAR PATTERN 2* (*CVP2*)[34] and *CLAVATA3/EMBRYO SURROUNDING REGION-RELATED 45 (CLE45)*[35,36] (Fig. 4e-g, Supplementary Fig. 5). *ALTERED PHLOEM DEVELOPMENT* (*APL*), a major phloem marker which inhibits xylem differentiation, was also detected in this region[37] (Fig. 4e). Transcripts related to phloem differentiation, including *CLE41*, *DOF5.1* and *LBD3* were enriched in the lower region of PC^{PP} (Fig. 4h-j, Supplementary Fig. 5). Strikingly, the arrangement in the UMAP plot, of the PC^{PP} cluster facing the PP

cluster (C10.2) and the PC^{XP} facing the XP clusters, is analogous to the morphological positioning. A detailed description of the procambium clusters is included in the Supplementary Text.

Two phloem parenchyma clusters

SWEET11 and SWEET12 efflux transporters had previously been reported to be expressed in the PP[8,38]. Sucrose released by the SWEETs into the apoplasm is taken up into the neighboring SE/CC via the sucrose/H^+ symporter SUC2/SUT1[6,39]. Interestingly, we identified two clusters, C10.2 (PP1) and C18.1 (PP2), specifically enriched for *SWEET11* and *SWEET12* (Fig. 3, Fig. 5a-f). Cells in the two PP clusters are enriched for transcripts related to transport processes, reflecting the roles of PP as a critical cell type required for loading diverse substrates into the phloem (Supplementary Tables 7, 9-11). We identified an additional member of the Clade III SWEET family, *SWEET13*, in the cells that expressed *SWEET11* and *SWEET12* (Fig. 5g-i). *SWEET13* transcripts show compensatory accumulation in *sweet11;sweet12* double knockout mutants, indicating redundant roles with SWEET11 and SWEET12[38]. Using a modified protocol from a recently developed confocal imaging method that enables identification of PP [8], we were able to validate the presence of SWEET11 and SWEET13 in the PP-cells in *pSWEET13:SWEET13-YFP* (Fig. 5p) and *pSWEET11:SWEET11-2A-GFP* lines (Fig. 5q,r).

UmamiT family members have been described as cellular exporters for amino acids[40]. We thus speculated that UmamiTs may play analogous roles for the efflux of amino acids from PP as the SWEETs do for sucrose. Consistent with our hypothesis, we found *UmamiT18/SIAR1* mRNA in PP (Figs 5j-l). Vascular expression in leaves is supported by *UmamiT18/SIAR1* transcriptional fusion lines[40]. In addition, transcripts for six other members of the UmamiT family (UmamiT12, 17, 20, 21, 28, 30) were enriched in the two PP clusters (Fig, 5m-o, Supplementary Fig. 6a-f, Supplementary Tables 7 and 11). Notably many of the PP-specific *UmamiT*s were coexpressed with each other as well as *SWEET11* and *12* (Supplementary Fig. 6g, Supplementary Table 12).

As many transcripts related to transport processes were specifically enriched in the PP clusters, and many of them were coregulated (Supplementary Table 12), this may indicate that they are subject to control by the

same transcriptional networks. We therefore searched for transcription factors that might be responsible for coregulation of the functionally related transporters. We identified multiple leucine zipper genes (bZIP) either specific to the PP clusters (*bZIP*6, *bZIP7*, *bZIP9*), or present in PP and other clusters (*TGA7*, *bZIP11*; Supplementary Fig. 7). We were able to confirm that *bZIP9* promoter activity was specific for the PP cells in the leaf vasculature, using a transcriptional fusion, *pbZIP9:GFP-GUS* (Fig. 6a-d). Strong GUS activity was also detected in cell types known to be involved in apoplasmic transport steps, such as the unloading zones of anthers and seeds, and the veins of petals, receptacles, ovules, transmitting tract, and funiculi (Supplementary Fig. 8). The cell specificity of bZIP9 is consistent with a possible role in the activation of target genes involved in transport process across different tissues. The nature of the separation of PP into two subclusters will require further analysis.

The companion cell cluster

Companion cells, which acquire carbon and nitrogen from the adjacent PP, but also maintain the functionality of the enucleate sieve elements, cluster separately from all other cell types. C15 was designated as CC based on the enrichment of transcripts for the sucrose/H^+ symporter *SUC2/SUT1*, the H^+-ATPase *AHA3,* and genes such as *FTIP* and *APL* (Fig. 3, Supplementary Fig. 3a). CCs were enriched for transcripts of various transporters, including the amino acid/H^+ symporter *AAP2* (ref.[41]), the potassium channel *KAT1* (ref.[42]), the hexose uniporters *SWEET1* and *SWEET4* (ref.[43]), and the tonoplast peptide transporter *PTR4/NPF8.4* (ref.[44]) (Supplementary Table 11). All these markers are also enriched in the CC translatome[45]. Notably, many genes involved in control of flowering were also enriched in CCs (Supplementary Table 3).

PP and CC cells undergo differentiation through distinct pathways

The clear separation of PP and CC in the UMAP was striking and indicates the presence of distinct differentiation pathways. The MYB coiled-coil-type transcription factor APL plays a key role for the definition of phloem identity[37]. In our datset, APL was preferentially expressed in CC, but also detected in the PC^{PP} cluster (Fig 4e and Supplementary Fig. 3a). As APL function is necessary for the development of the SECC complex, one may propose two hypotheses: (i) APL serves as a master regulator of all phloem

cells, or (ii) PP develops independently of the SECC differentiation. While *apl* mutants are characterized by drastic reduction of CC marker *SUC2* [37], *apl* retains expression of multiple PP markers (Fig. 7b); PP marker transcripts were even > fourfold higher in the *apl* mutant (Fig. 7a). Whether the increase of PP-marker transcripts in *apl* is due to a compensatory mechanism in which APL represses PP differentiation, as suggested for xylem differentiation[37], remains to be elucidated.

Unique and complementary metabolic landscapes of PP and CC

Amino acid transporters of the AAP and UmamiT families are relatively non-selective and transport many of the proteogenic and other amino acids[28,46]. One may therefore assume that the translocation of most amino acids is similar and that relative amino acid levels are mainly determined by the relative rates of biosynthesis, that the amino acids all enter the translocation stream in similar ways and that the relative levels do not change substantially during translocation. However, labeling studies have shown that amino acids behave very differently, with some being effectively metabolized along the path of source-to-sink partitioning, while other stay largely unmetabolized[47]. Surprisingly, the amino acid distribution in stems is also varying for different amino acids[48]. These phenomena might be explained by differential distribution of metabolic activities in different vascular cell types. We therefore carried out a pathway activity analysis to define a pathway activity score (PAS) that quantifies the average expression of the pathway's genes in one cell type relative to the other cell types[49]. The PAS values of the CC and PP were strikingly different for both amino acid biosynthetic and degradation pathways (Fig. 8). While the activity of biosynthetic amino acid pathways was low in CC, PP-containing clusters showed elevated metabolic activity. A comprehensive analysis of pathway activities across all clusters revealed many other interesting features unique to specific cell types. For instance, the epidermis cluster (C13) was enriched with biosynthetic activities for wax esters, cuticular wax, the suberin monomer and very long chain fatty acids. These substances function as coatings in the epidermis, serving as a moisture barrier and protecting plants from pathogens. The PP-including cluster, C18, showed high activity of hormone pathways such as ABA, ethylene, JA, and GA, and the BS and XP clusters (C4) and the two PP-including clusters (C10 and C18) were enriched for glucosinolate biosynthesis activity (Supplementary Text,

Supplementary Figs. 9 and 10). C19 may represent so-called S-cells, cell likely involved in defense responses, based on the enrichment of programmed cell death pathways and PAS values for insect chewing-induced glucosinolate breakdown[50] (Supplementary Table 13, Supplementary Text). The two PP clusters (C10, C18) showed high PAS values for callose biosynthesis, consistent with callose deposition in PP transfer cells[51]. We also provide a PAS analysis across all cell types that is not discussed further here (Supplementary Fig 10, Supplementary Text).

Cell-type specific expression of plasmodesmatal proteins

Plasmodesmata (PD) are highly complex channels that interconnect plant cells, likely transporting solutes, metabolites, small RNAs and proteins. Different cell types have unique types of plasmodesmata, including that which connects CC to enucleate sieve elements to supply all components necessary for function. The PDs typically are branched on the CC side and have a single pore on the sieve element side. We here found that transcripts of PD genes such as the *PLAMODESMATA-LOCATED PROTEIN* (*PDLP*)s and *MULTIPLE C2 DOMAINS AND TRNAMEMBRANE REGION PROTEIN (MCTP*)s showed distinct expression patterns in different cell types (Fig. 9a-d, Supplementary Fig. 11a,b)[52,53]. For example, *PDLP6*, *7,* and *8* transcripts were found in PP and CC, while *PDLP2* and *3* transcripts were present in mesophyll cells (Fig. 9a-d, Supplementary Fig. 11a). The cell-type specificity of *PDLP*s was correlated with their phylogenetic relationships (Fig. 9e). Our results are consistent with data from GUS reporter fusions for the *PDLP7* and *8* promoters[54]. *MCTP1* and *3* transcripts were mainly enriched in the vasculature (Supplementary Fig. 11b). In particular, *MCTP1* transcript was specifically enriched in CC, consistent with a role in trafficking the florigen protein FLOWERING LOCUS T (FT), from companion cell to sieve elements[55]. In comparison, *MCTP4*, *MCTP6* and *MCTP15* are ubiquitously expressed in vascular and mesophyll cells (Supplementary Fig. 11b). Overall, our data supports the concept of PD-type specific assembly of PDs.

DISCUSSION

Despite the advances in scRNA-seq technologies, application to plant cells still faces the challenge of removing cell walls to allow the release of individual cells and the penetration of the buffers into cells. Recent studies (using Arabidopsis, rice, as well as maize aerial tissues) clearly demonstrate the difficulty of capturing vascular cell types. For example, a key cell type in the vasculature, the PP, was not identified in any of the recently published scRNA-seq data from roots[9–13]. Here, we systematically optimized protoplast isolation protocols to enrich vascular cell types and produced a single cell transcriptome and metabolic activity score atlas that covers essentially all known cell types in the Arabidopsis leaf. The scRNA-seq confirmed that except for trichomes, abaxial epidermis and guard cells which were intentionally removed, all known nucleus-containing cells of the leaf were represented in the dataset. In particular, all cells from the leaf vasculature were identified.

The vascular cells had identities clearly distinct from those of the epidermis, guard cells and mesophyll. The bundle sheath formed a supercluster, together with all vascular cells including the vascular meristem, except the companion cells (CC). A major finding within this atlas was that the kinship relation of vascular cells was highly similar to the actual morphology of the vasculature, with the exception of the CC, which formed a unique island separate from BS, xylem, procambium and the phloem parenchyma. The arrangement of the XP-PC^{XP}-PC^{PP}-PP clusters in the UMAP plot reflected a potential developmental trajectory, in which the meristematic cells are localized in the center of the cluster and the surrounding cells differentiate and acquire distinct identities. A future pseudotime trajectory analysis will allow us to better understand the transition from meristematic cell to differentiated phloem or xylem cells types. Some clusters showed gradients, indicating a transition, in which transcriptional modules (for example, for xylem identity) decreased in favor of phloem modules. One example is the PC, in which cells closer to the xylem shared some xylem properties, while those closer to PP shared PP properties. A similar behavior was seen for the VP. It is conceivable that the well-studied dorsoventral cues, or cues from neighboring cells, are responsible for these gradients.

From their positioning inside the phloem, one may naively have expected the PP and CC to cluster together.

CC are unique since they have to fulfil their own tasks, e.g. import sucrose from PP, and at the same time maintain the function of the adjacent enucleate sieve elements, living cells that act as conduits for assimilate translocation[56]. Based on this dual role, it is possibly not surprising that they form such a distinct island. Whether PP and CC derive from a common ancestor remains unclear since the ontogeny of PP is unknown. The ontogenesis of CC is much better understood[37]. SE/CC mother cells divide asymmetrically to produce CC and SE. The APL transcription factor is a master regulator for SE/CC development, and a repressor of xylem identity[37]. Based on our data, it seems unlikely that APL is responsible for driving PP ontogeny but may implicate alternative pathways for PP differentiation.

A major discovery was the assignment of Clusters 10 and 18 as PP, providing first insights into the PP transcriptome. The PP has essential roles in sucrose transfer to the SE/CC, but also likely many other functions in transport, metabolism and signaling. Using *SWEET11* and *12* as markers, two distinct clusters were identified, C10.2 and C18.1. It will require more careful analyses to determine if the two clusters represent spatially different cells types or developmental trajectories. *SWEET13* is a gene that may act in a compensatory role, as evidenced by higher mRNA levels in *sweet11;12* mutants. Here we detected *SWEET13* in the same cells as *SWEET11* and *12* (ref. [38]). Notably, in a parallel study we found that while in main veins and rank-1 intermediate veins of maize, the orthologs in maize, named *ZmSWEET13a, b* and *c*, are likely also expressed in PP, in the C4 specific rank-2 intermediate veins that are mainly responsible for phloem loading, the three *ZmSWEET13*s are not in PP, but in two abaxial bundle sheath cells[57]. These data indicated to us that maize uses a different path for phloem loading of sucrose as compared to for example Arabidopsis or potato[58]. In addition to the clade III SWEETs, scRNA-seq provided extensive insights into other genes enriched in PP, in particular identifying transcripts of seven members of the UmamiT amino acid transporter family. UmamiTs are rather non-selective transporters involved at sites where cellular amino acid efflux is required. For example, *UmamiT18/SIAR1* transcripts, similar to *SWEET11* and *12*, were detected in the chalazal region of developing seed[40,59]. Knockout mutants showed reduced accumulation of amino acids in seeds, likely due to both a reduction in efflux from leaves and reduced efflux from the chalaza[40]. Of note, the *SWEET*s and *UmamiT*s showed high coexpression indices. One may thus hypothesize that the genes share transcriptional

control, and thus it will be interesting to analyze whether common transcription factors binding sites are present in the PP-specific genes. SWEETs and SUTs seem to act as a pair, one responsible for sucrose efflux from PP, the other for active import into the SE/CC. UmamiTs also seem to act in pairs, with UmamiTs in PP and AAP amino acid H^+/symporters[60] including *AAP2*, *4* and *5* in the CC (Supplementary Fig. 14). These complementary functions are consistent with the clear separation of the clusters in the UMAP plots. A striking result from the comparison of PP and CC was that their metabolism was also highly differentiated. In particular, we found major differences regarding amino acid metabolic pathways. Both isotope labeling studies as well as amino acid localization by 2D-NMR had indicated that amino acids behave very differently regarding entry into metabolism along the translocation pathway and entry into the phloem[47,48]. This difference could thus likely be explained by the metabolic activities along the path, rather than their non-selective transporters.

Cell type-specific metabolic pathway analysis revealed many other interesting aspects. For example, hormone metabolism varied between cell types. Cell types responsible for hormones biosynthesis are largely unknown. The metabolic analysis provides a map that may guide identification of hormone biosynthesis and transport pathways in leaves. For instance, high activities of ABA, ethylene, JA, and GA biosynthesis pathways were detected in C18 (which includes the PP), consistent with the high number ABA, JA, and GA transporters in the phloem[61–64]. As most transporters show functional redundancy and display diverse substrate specificity, this dataset serves as a source to identify cell type-specific redundant family members for the generation of multiple mutants, to eliminate or verify interacting partners, and to identify yet -unknown transporters.

Besides the insights into both metabolism and into apoplasmic transport pathways, the study also showed that cell types with unique types of plasmodesmata express particular paralogs of plasmodesmata-specific proteins, such as PDLPs or MCTPs. The combined analysis of sym- and apoplasmic fluxes of ions, metabolites and signaling molecules at the cellular level will likely enable a much better understanding of the physiology of the leaf.

In summary, scRNA-seq enabled us to identify unique and distinct features of the different vascular cell types present the leaf. Through transcriptomic and metabolic pathway analyses at the single cell level, we identified potential roles of PP not only in the transport of sugars, but also in amino acid transport. Importantly, we also identified unexpected roles of PP in hormone biosynthesis and defense-related responses. The information provided in this study provides key resources to develop strategies influencing the flux of ions, metabolites and signals.

METHODS

Enrichment of vascular protoplasts. Protoplasts were isolated from mature leaves of 6-weeks-old Arabidopsis Col-0 plants grown under short-day (8 h light / 16 h dark) conditions at a PAR of 60 µmol m^{-2} s^{-1}. For protoplast isolation, the tape-sandwich method[15] was modified and applied for removal of the abaxial epidermis, guard cells and trichomes. The adaxial side of the fully developed leaves was stabilized by placing on the time tape, and the abaxial side was adhered to the 3M Magic tape. The abaxial epidermis was removed by pulling off the 3 M Magic tape. Two cuts were made on each side of the major vein of the peeled leaves using a razor blade (Swann-Morton, Sheffield). Seven to nine abaxial epidermis-peeled and cut leaves attached to time tape were immediately immersed in the petri dish containing 15 mL freshly prepared protoplast isolation solution (1% Cellulase Onuzuka R-10 (Duchefa, Haarlem), 0.3% macerozyme R-10, (Duchefa, Haarlem), 0.6 M Mannitol, 20 mM MES pH 5.7, 20 mM KCL, 1 mM DTT, 10 mM $CaCl_2$, and 0.1 % BSA). Dithiothreitol (DTT) and bovine serum albumin (BSA) were added to the enzyme solution to protect the protoplasts. Leaves were shaken at 30 rpm on a platform shaker for 2 hours. The release of the protoplasts was monitored every 30 min by checking released cells under the microscope or by monitoring what was left on the time tape. After confirming the release of the protoplasts into the solution, 10 mL of wash buffer (0.6 M Mannitol, 20 mM MES pH 5.7, 20 mM KCl, 1 mM DTT, 10 mM $CaCl_2$, and 0.1 % BSA) was slowly added to the petri dish containing the protoplasts. The solution was filtered into a round bottom 20 mL tube using a 70 µm pore size filter (Corning, New York). The protoplast solution was centrifuged at 100 x *g* for 3 min in a swinging rotor. The protoplasts were washed four times with 20 mL washing buffer. After the final wash step, protoplasts were slowly resuspended in 1 mL wash buffer and gently filtered twice using a 40 µm Flowmi cell strainer (Bel-Art SP Scienceware, New Jersey). The number of protoplasts was counted with the C-Chip Neubauer improved hemocytometer (NanoEnTek, Seoul) under a light microscope (Leica VT1000, Wetzlar). The viability of protoplasts was determined using trypan blue solution (Gibco; Thermo Fisher Scientific, Massachusetts).

Quantitative reverse transcription (RT-qPCR). Total RNA was extracted using the RNeasy Kit (Qiagen, Hilden). cDNA synthesis and gDNA removal steps were performed using QuantiTect Reverse Transcription Kit (Qiagen, Hilden), qPCR was performed on Stratagene Mx3000P (Agilent Technologies, California) using the Lightcycler 480 SYBR Green I Master Mix (Roche, Penzberg). Transcript levels were quantified using the relative standard curve method. Values were normalized to the level of the internal control, *UBQ10*. Primers used for RT-qPCR are listed in Supplementary Table 15. For RT-qPCR of *apl* mutants, segregating seeds from heterozygous parents were sown on MS media. RNA was extracted using 2-weeks-old plants grown under LD conditions.

Single cell RNA-seq library preparation and sequencing. Two biological replicates were performed with the aim of capturing ~7,000 leaf protoplasts for each replicate. Freshly isolated protoplasts were adjusted to 700-900 cells/μL and loaded into the 10X Genomics Chromium single cell microfluidics device according to the Single Cell 3' Reagent Kit v2 protocol (10x Genomics, California). Eleven cycles were used for cDNA amplification and 12 cycles were used for final PCR amplification of the adapter-ligated libraries. The quality and size of the final library was verified on a DNA High Sensitivity Bioanalyzer Chip (Agilent Technologies, California), and libraries were quantified using the NEBNext Library Quantification Kit for Illumina (New England Biolabs, Massachusetts). scRNA-seq library sequencing was performed on a NextSeq platform (Illumina Inc, California), using the sequencing parameters 26,8,0,98 (c.ATG, Tübingen).

Generation of single cell expression matrices. Reads were aligned to the *Arabidopsis thaliana* reference genome (Araport 11) using Cell Ranger 3.0.2 (10X Genomics, California) with default parameters. The output files for the two replicates were aggregated into one gene-cell expression matrix using Cell Ranger aggregate with the mapped read depth normalization option.

Dimensionality reduction, UMAP visualization, cell clustering analysis, and correlation analysis. The Seurat R package (version 3.1.0)[17,65] was used for dimensionality reduction analysis. The SCTransform option was used for normalization, scaling the data and finding variable genes using default parameters[66]. During normalization, potential variation due to mitochondrial mapping percentage was removed. We did

not remove rRNA before sample preparation and did not filter cells with higher rRNA transcript levels, since rRNA levels can vary among cells. Fifty principal components (PCs) were selected as input for a graph-based approach to cluster cells by cell type using a resolution value of 0.8 in all clustering analyses. Uniform Manifold Approximation and Projection (UMAP) dimensional reduction[18] was used for two-dimensional visualization using ten PCs, 30 neighboring points and a minimum distance of 0.1. Subclustering was performed using the same parameters. For the correlation analysis between single cell replicates across individual clusters, the average expression of cells within a cluster was calculated and the Pearson-correlation coefficient was determined.

Identification of Differentially Expressed Genes and Cluster-Specific Marker Genes. Genes differentially expressed across clusters or subclusters were identified by comparing average transcript levels in cells of a given cluster to that of cells in all other clusters using the Seurat package likelihood ratio test (Bimod). The following cutoffs were applied: average expression difference ≥0.25 natural Log and q <0.01. Cluster-specific marker genes were selected from among the differentially expressed genes based on the criteria that marker genes must be expressed in >10% of cells within the cluster (PCT1), and <10% of cells across all other clusters (PCT2).

Bulk RNA-seq library preparation and sequencing. Total RNA was extracted from leaves (not protoplasted) and leaf protoplasts isolated using the same method for the single cell sequencing using the RNeasy Kit (Qiagen, Hilden). On column DNase treatment was performed to remove residual gDNA using the RNase-free DNase kit (Qiagen, Hilden) following manufacturer recommendations. Two biological replicates were made for leaf and leaf protoplast samples. The integrity of the RNA was confirmed using Agilent RNA 6000 Nano Chip (Agilent Technologies, California) and LabChip GX (PerkinElmer, Massachusetts). RNA concentration was measured using the Qubit Fluorometer using the RNA broad range quantification kit (Thermo Fisher, Massachusetts). For mRNA poly-A enrichment, 5 µg of total RNA was purified using the Poly(A) mRNA Magnetic Isolation Module (New England Biolabs, Massachusetts). Libraries were constructed using the ULTRA II directional library kit (New England Biolab, Massachusetts),

and size selection was done using SPRI beads (New England Biolab, Massachusetts) following the manufacturer manual with the following exceptions: 7 min of fragmentation time and 26.5 and 10 µL SPRI beads pre-PCR were used to enrich ~400 bp inserts. Library amplification included 10 PCR cycles, and 0.7 volumes of (35 µL) of SPRI beads were used for post-PCR purification. QC-tested libraries (Agilent Technologies, California) were sequenced on an Illumina HiSeq 2500 lane with 150 bp paired-end (Novogene, Beijing).

Bulk RNA-seq analysis. Paired-end reads (150 bp) were aligned to the *Arabidopsis thaliana* reference genome (Araport11) using STAR[67] (maximum intron length of 2 kbp). Differential expression analysis was carried out in R (v3.6.1) using Bioconductor (v3.9) and DESeq2 (v1.24) (absolute Log2FC ≥ 1 and q value < 0.05). For correlation analysis of gene expression between protoplasted and non protoplasted bulk tissues, the Log2 (mean FPKM+1) expression values were calculated for each gene. Pearson-correlation coefficient was determined in R.

Pathway activities in different cell types. We followed the formulation introduced in Xiao *et al.*[49] to calculate a pathway activity score, which depends on the mRNA level of its constituent genes. The mRNA count of gene i in cell k was denoted as $g_{i,k}$. We first normalized the mRNA count of a gene in a cell by the average for all genes in the cell, and denoted this normalized level as $g'_{i,k}$. The mean transcript level $E_{i,j}$ of gene i in cell type j is then defined as the mean $g'_{i,k}$ over all cells of that type, $E_{i,j} = \frac{1}{n_j}\sum_{k=1}^{n_j} g'_{i,k}$, where n_j is the number of cells classified as cell type j, and k is the index for individual cells. $E_{i,j}$ is normalized by the average transcript level of gene i across all cell types to become the relative transcript level $r_{i,j}$ of gene i in cell type j: $r_{i,j} = E_{i,j} / \left(\frac{1}{N}\sum_{a=1}^{N} E_{i,a}\right)$, where N is the total number of cell types. The pathway activity score (PAS) of pathway t in cell type j, denoted as $p_{t,j}$, is then a weighted average of the relative transcript levels across the pathway genes: $p_{t,j} = \frac{\sum_{i=1}^{m_t} w_i r_{i,j}}{\sum_{i=1}^{m_t} w_i}$; here, m_t is the number of genes in pathway t, and the weight w_i of gene i is defined as the reciprocal of the number of pathways that include gene i, to ensure a stronger influence of pathway-specific genes. As the relative mRNA levels $r_{i,j}$ are centered around 1, the same is true

for the pathway activity $p_{t,j}$, with $p_{t,j}$ <1 corresponding to underrepresentation of pathway *t* in cell type *j* relative to the pathway's activity across all cell types; conversely, $p_{t,j}$ >1 indicates a higher than average activity in cell type *j*. To assess the statistical significance of a $p_{t,j}$ value, we performed a permutation test, shuffling the cell type labels of the genes a thousand times to simulate the null distribution of $p_{t,j}$ under the assumption of no systematic cell type specific pathway activity; we defined an empirical *p*-value by comparing $p_{t,j}$ to this null distribution. AraCyc pathway lists[68] used for the analysis can be found in Supplementary Table 14.

Generation of reporter lines. For the generation of *pbZIP9:GFP-GUS* lines, a 2,289 bp fragment of the *bZIP9* gene promoter was amplified using bZIP9pro attB1 and bZIP9pro attB2 primers using Col-0 genomic DNA as template. The corresponding PCR fragment was purified and used for GATEWAY BP reaction into pDONR221 and cloned into the destination vector pBGWFS7,0 through LR reaction. For generating *pSWEET11:SWEET11-2A-GFP-GUS* lines, a 4,784 fragment consisting of promoter and SWEET11 genomic region including all exons and introns was amplified using SWEET11-2A-attB1 and SWEET11-2A-attB2 primers. The SWEET11-2A-attB2 reverse primer contained the 2A cleavage sequence. The genomic SWEET11 with the 2A cleavage site was cloned into pDONR221 and subcloned into the pBGWFS7,0 vector through LR reaction. To generate *pSWEET13:SWEET13-YFP*, a 3,941 bp fragment including SWEET13 promoter and its genomic region was amplified using SWEET13attB1 and SWEET13attB2 primers and cloned into the donor vector pDONR221-f1 by BP reaction. Subsequently, the fragment was sub-cloned into a gateway-compatible vector, pEG-TW1[69] to generate pSWEET13:SWEET13-YPF construct by LR reaction. Transformation of plants was performed using the floral dip method[70]. Primers used for amplification are listed in Supplementary Table 15.

GUS histochemistry. GUS staining was performed as described with minor modifications[71]. Tissues were fixed with 90% ice-cold acetone. After applying vacuum for 10 min, acetone was removed and replaced by prestaining solution (1 mM EDTA, 5 mM potassium ferricyanide, 5 mM potassium ferrocyanide, 100 mM

sodium phosphate (pH 7.0), 1% Triton-X-100). After 10 min vacuum, the prestaining solution was replaced with staining solution containing 1 mM EDTA, 5 mM potassium ferricyanide, 5 mM potassium ferrocyanide, 100 mM sodium phosphate (pH 7.0), 1% Triton-X-100, and 2 mM X-Gluc and further vacuum infiltrated for 15 min in the dark. The tissues in staining solutions containing X-Gluc were incubated at 37 ºC in the dark for 4 hours. Ethanol series were performed from 25% to 70% ethanol in 30 min steps.

Sample preparation for imaging leaf vasculature. Rosette leaves were excised by cutting the leaf petiole from 5 weeks old plants grown under SD conditions. Double-sided tape was used to attach the petiole and the upper lamina of the leaf on the slide glass (abaxial side facing upward, as in the tape-sandwich method). The abaxial epidermis was peeled using the 3M Magic tape and immediately covered with water. The region of interest was excised with a razor blade and moved to a new slide glass. Samples were applied with FM4-64FX (Sigma-Aldrich, Missouri) (5 μg/ml) for 5 min for staining the cell membrane and imaged immediately. PP-cells were identified based on the cell size and chloroplast organization as described[8].

Confocal imaging. Fluorescence images were captured using a Leica TCS SP8 confocal microscope with a 20x or 40x objective with water immersion. GFP, YFP, FM4-64FX, and chlorophyll autofluorescence signals were acquired using the following settings: GFP, excitation 488 nm (white-light laser) and emission 492-552 nm; YFP, excitation 514 nm and emission 510-565 nm; FM4-64FX, excitation 561 nm and emission 599–680 nm; chlorophyll autofluorescence, excitation 638 nm and emission 645-738 nm.

503 **Reporting Summary.** Further information on research design is available in the Nature Research Reporting
504 Summary linked to this article.

505 **Data availability**

506 The raw data that support the findings of this study are available from the corresponding author upon
507 reasonable request. All sequencing data have been deposited in the Gene Expression Omnibus GEO
508 (www.ncbi.nlm.nih.gov/geo/) under the accession number GEO X and The Single Cell Expression Atlas at
509 EMBL-EBI (www.ebi.ac.ik/gxa/sc/home).

REFERENCES

1. Haritatos, E., Medville, R. & Turgeon, R. Minor vein structure and sugar transport in *Arabidopsis thaliana*. *Planta* **211**, 105–11 (2000).

2. Kang, J. & Dengler, N. Vein pattern development in adult leaves of *Arabidopsis thaliana*. *Int. J. Plant Sci.* **165**, 231–242 (2004).

3. Nguyen, C. T., Kurenda, A., Stolz, S., Chételat, A. & Farmer, E. E. Identification of cell populations necessary for leaf-to-leaf electrical signaling in a wounded plant. *Proc Natl Acad Sci USA* **115**, 10178 (2018).

4. Arun Chinnappa, K. S., Nguyen, T. T. S., Hou, J., Wu, Y. & McCurdy, D. W. Phloem parenchyma transfer cells in *Arabidopsis* - an experimental system to identify transcriptional regulators of wall ingrowth formation. *Front Plant Sci* **4**, 102 (2013).

5. Edwards, J. *et al.* GIGANTEA is a component of a regulatory pathway determining wall ingrowth deposition in phloem parenchyma transfer cells of *Arabidopsis thaliana*. *Plant J.* **63**, 651–661 (2010).

6. Riesmeier, J. W., Willmitzer, L. & Frommer, W. B. Evidence for an essential role of the sucrose transporter in phloem loading and assimilate partitioning. *EMBO J.* **13**, 1–7 (1994).

7. Chen, L. Q. *et al.* Sucrose efflux mediated by SWEET proteins as a key step for phloem transport. *Science* **335**, 207 (2012).

8. Cayla, T., Le Hir, R. & Dinant, S. Live-cell imaging of fluorescently tagged phloem proteins with confocal microscopy. *Methods Mol. Biol.* **2014**, 95–108 (2019).

9. Denyer, T. *et al.* Spatiotemporal developmental trajectories in the *Arabidopsis* root revealed using high-throughput single-cell RNA sequencing. *Dev. Cell* **48**, 840-852.e5 (2019).

10. Ryu, K. H., Huang, L., Kang, H. M. & Schiefelbein, J. Single-cell RNA sequencing resolves molecular relationships among individual plant cells. *Plant Physiol.* **179**, 1444–1456 (2019).

11. Zhang, T.-Q., Xu, Z.-G., Shang, G.-D. & Wang, J.-W. A single-cell RNA sequencing profiles the developmental landscape of Arabidopsis root. *Mol Plant* **12**, 648–660 (2019).

12. Shulse, C. N. *et al.* High-throughput single-cell transcriptome profiling of plant cell types. *Cell Rep.* **27**, 2241-2247.e4 (2019).

13. Jean-Baptiste, K. *et al.* Dynamics of Gene Expression in Single Root Cells of Arabidopsis thaliana. *Plant Cell* **31**, 993 (2019).

14. Birnbaum, K. *et al.* A gene expression map of the *Arabidopsis* root. *Science* **302**, 1956–60 (2003).

15. Wu, F.-H. *et al.* Tape-*Arabidopsis* Sandwich - a simpler *Arabidopsis* protoplast isolation method. *Plant Meth.* **5**, 16 (2009).

16. Radoeva, T., ten Hove, C. A., Saiga, S. & Weijers, D. Molecular characterization of *Arabidopsis* GAL4/UAS enhancer trap lines identifies novel cell-type-specific promoters. *Plant Physiol.* **171**, 1169 (2016).

17. Satija, R., Farrell, J. A., Gennert, D., Schier, A. F. & Regev, A. Spatial reconstruction of single-cell gene expression data. *Nat. Biotech.* **33**, 495–502 (2015).

18. McInnes, L., Healy, J. & Melville, J. UMAP: uniform manifold approximation and projection for dimension reduction. *arXiv* **eprint arXiv:1802.03426**, (2018).

19. Sawchuk, M. G., Donner, T. J., Head, P. & Scarpella, E. Unique and overlapping expression patterns among members of photosynthesis-associated nuclear gene families in *Arabidopsis*. *Plant Physiol.* **148**, 1908 (2008).

20. Endo, M., Shimizu, H., Nohales, M. A., Araki, T. & Kay, S. A. Tissue-specific clocks in *Arabidopsis* show asymmetric coupling. *Nature* **515**, 419–422 (2014).

21. Uemoto, K., Araki, T. & Endo, M. Isolation of Arabidopsis palisade and spongy mesophyll cells. *Methods Mol. Biol.* **1830**, 141–148 (2018).

22. Takada, S., Takada, N. & Yoshida, A. *ATML1* promotes epidermal cell differentiation in *Arabidopsis* shoots. *Development* **140**, 1919 (2013).

23. Bürkle, L. *et al.* Transport of cytokinins mediated by purine transporters of the PUP family expressed in phloem, hydathodes, and pollen of Arabidopsis. *Plant J.* **34**, 13–26 (2003).

24. Haritatos, E., Medville, R. & Turgeon, R. Minor vein structure and sugar transport in *Arabidopsis thaliana*. *Planta* **211**, 105–11 (2000).

25. Endo, A. *et al.* Drought induction of *Arabidopsis* 9-cis-epoxycarotenoid dioxygenase occurs in vascular parenchyma cells. *Plant Physiol* **147**, 1984–1993 (2008).

26. Pilot, G. *et al.* Overexpression of GLUTAMINE DUMPER1 leads to hypersecretion of glutamine from hydathodes of Arabidopsis leaves. *Plant Cell* **16**, 1827–40 (2004).

27. Okumoto, S. *et al.* High affinity amino acid transporters specifically expressed in xylem parenchyma and developing seeds of Arabidopsis. *Journal of Biological Chemistry* **277**, 45338–45346 (2002).

28. Dinkeloo, K., Boyd, S. & Pilot, G. Update on amino acid transporter functions and on possible amino acid sensing mechanisms in plants. *Sem Cell Dev Biol* **74**, 105–113 (2018).

29. Madsen, S. R., Olsen, C. E., Nour-Eldin, H. H. & Halkier, B. A. Elucidating the role of transport processes in leaf glucosinolate distribution. *Plant Physiol.* **166**, 1450 (2014).

30. Nour-Eldin, H. H. *et al.* NRT/PTR transporters are essential for translocation of glucosinolate defence compounds to seeds. *Nature* **488**, 531–534 (2012).

31. Sanchez, P., Nehlin, L. & Greb, T. From thin to thick: major transitions during stem development. *Trends Plant Sci* **17**, 113–121 (2012).

32. Elo, A., Immanen, J., Nieminen, K. & Helariutta, Y. Stem cell function during plant vascular development. *Sem. Cell Dev. Biol.* **20**, 1097–1106 (2009).

578 33. Baima, S. *et al.* The *Arabidopsis* ATHB-8 HD-zip protein acts as a differentiation-promoting
579 transcription factor of the vascular meristems. *Plant Physiol* **126**, 643–655 (2001).

580 34. Rodriguez-Villalon, A., Gujas, B., van Wijk, R., Munnik, T. & Hardtke, C. S. Primary root protophloem
581 differentiation requires balanced phosphatidylinositol-4,5-biphosphate levels and systemically affects
582 root branching. *Development* **142**, 1437 (2015).

583 35. Gujas, B. *et al.* A reservoir of pluripotent phloem cells safeguards the linear developmental trajectory of
584 protophloem sieve elements. *Curr. Biol.* **30**, 755-766.e4 (2020).

585 36. Rodriguez-Villalon, A. *et al.* Molecular genetic framework for protophloem formation. *Proc Natl Acad*
586 *Sci USA* **111**, 11551 (2014).

587 37. Bonke, M., Thitamadee, S., Mähönen, A. P., Hauser, M.-T. & Helariutta, Y. APL regulates vascular
588 tissue identity in *Arabidopsis*. *Nature* **426**, 181–186 (2003).

589 38. Chen, L. Q. *et al.* Sucrose efflux mediated by SWEET proteins as a key step for phloem transport. *Science*
590 **335**, 207–11 (2012).

591 39. Gottwald, J. R., Krysan, P. J., Young, J. C., Evert, R. F. & Sussman, M. R. Genetic evidence for the *in*
592 *planta* role of phloem-specific plasma membrane sucrose transporters. *Proc Natl Acad Sci USA* **97**,
593 13979 (2000).

594 40. Ladwig, F. *et al.* Siliques are Red1 from Arabidopsis acts as a bidirectional amino acid transporter that
595 is crucial for the amino acid homeostasis of siliques. *Plant Physiol.* **158**, 1643–55 (2012).

596 41. Zhang, L. *et al.* Altered xylem-phloem transfer of amino acids affects metabolism and leads to increased
597 seed yield and oil content in *Arabidopsis*. *Plant Cell* **22**, 3603–3620 (2010).

598 42. Schachtman, D. P., Schroeder, J. I., Lucas, W. J., Anderson, J. A. & Gaber, R. F. Expression of an inward-
599 rectifying potassium channel by the *Arabidopsis* KAT1 cDNA. *Science* **258**, 1654–1658 (1992).

600 43. Chen, L. Q. *et al.* Sugar transporters for intercellular exchange and nutrition of pathogens. *Nature* **468**,
601 527–532 (2010).

602 44. Weichert, A. *et al.* AtPTR4 and AtPTR6 are differentially expressed, tonoplast-localized members of the
603 peptide transporter/nitrate transporter 1 (PTR/NRT1) family. *Planta* **235**, 311–323 (2012).

604 45. Mustroph, A. *et al.* Profiling translatomes of discrete cell populations resolves altered cellular priorities
605 during hypoxia in Arabidopsis. *Proc Natl Acad Sci USA* **106**, 18843–8 (2009).

606 46. Fischer, W. N., Kwart, M., Hummel, S. & Frommer, W. B. Substrate specificity and expression profile
607 of amino acid transporters (AAPs) in Arabidopsis. *Journal of Biological Chemistry* **270**, 16315–16320
608 (1995).

609 47. Atkins, C. A. Biochemical aspects of assimilate transfers along the phloem path: N-solutes in lupins.
610 *Austr. J. Plant Physiol.* **27**, 531–537 (2000).

611 48. Metzler, A. *et al.* Plant histochemistry by correlation peak imaging. *Proc. Natl. Acad. Sci. USA* **92**,
612 11912–5 (1995).

613 49. Xiao, Z., Dai, Z. & Locasale, J. W. Metabolic landscape of the tumor microenvironment at single cell
614 resolution. *Nature Communications* **10**, 3763 (2019).

615 50. Koroleva, O. A., Gibson, T. M., Cramer, R. & Stain, C. Glucosinolate-accumulating S-cells in
616 *Arabidopsis* leaves and flower stalks undergo programmed cell death at early stages of differentiation.
617 *Plant J.* **64**, 456–469 (2010).

618 51. Maeda, H., Song, W., Sage, T. & DellaPenna, D. Role of callose synthases in transfer cell wall
619 development in tocopherol deficient Arabidopsis mutants. *Frontiers in Plant Science* **5**, 46 (2014).

620 52. Lee, J.-Y. *et al.* A plasmodesmata-localized protein mediates crosstalk between cell-to-cell
621 communication and innate immunity in Arabidopsis. *Plant Cell* **23**, 3353–3373 (2011).

622 53. Brault, M. L. *et al.* Multiple C2 domains and transmembrane region proteins (MCTPs) tether membranes
623 at plasmodesmata. *EMBO Rep.* **20**, e47182 (2019).

624 54. Tanvir, Z. Expression domain analysis of four members of the plasmodesmata-localized protein family
625 in Arabidopsis. (University of Delaware, 2016).

626 55. Liu, L. *et al.* FTIP1 Is an essential regulator required for florigen transport. *PLoS Biol.* **10**, e1001313
627 (2012).

628 56. Bel, A. J. E. van & Knoblauch, M. Sieve element and companion cell: the story of the comatose patient
629 and the hyperactive nurse. *Funct. Plant Biol.* **27**, 477–487 (2000).

630 57. Bezrutczyk, M. *et al.* Phloem loading via the abaxial bundle sheath cells in maize leaves. *Nat. Plants*
631 **submitted**,.

632 58. Kühn, C., Franceschi, V. R., Schulz, A., Lemoine, R. & Frommer, W. B. Macromolecular trafficking
633 indicated by localization and turnover of sucrose transporters in enucleate sieve elements. *Science* **275**,
634 1298–300 (1997).

635 59. Chen, L. Q. *et al.* A cascade of sequentially expressed sucrose transporters in the seed coat and
636 endosperm provides nutrition for the *Arabidopsis* embryo. *Plant Cell* **27**, 607 (2015).

637 60. Fischer, W.-N. *et al.* Amino acid transport in plants. *Trends Plant Sci.* **3**, 188–195 (1998).

638 61. Kuromori, T., Sugimoto, E. & Shinozaki, K. Intertissue signal transfer of abscisic acid from vascular
639 cells to guard cells. *Plant Physiol.* **164**, 1587 (2014).

640 62. Kanno, Y. *et al.* AtSWEET13 and AtSWEET14 regulate gibberellin-mediated physiological processes.
641 *Nat. Comm.* **7**, 13245 (2016).

642 63. Ye, Z.-W. *et al.* Arabidopsis acyl-CoA-binding protein ACBP6 localizes in the phloem and affects
643 jasmonate composition. *Plant Mol. Biol.* **92**, 717–730 (2016).

644 64. Nguyen, C. T., Martinoia, E. & Farmer, E. E. Emerging jasmonate transporters. *Mol Plant* **10**, 659–661
645 (2017).

646 65. Butler, A., Hoffman, P., Smibert, P., Papalexi, E. & Satija, R. Integrating single-cell transcriptomic data
647 across different conditions, technologies, and species. *Nat Biotech* **36**, 411–420 (2018).

66. Hafemeister, C. & Satija, R. Normalization and variance stabilization of single-cell RNA-seq data using regularized negative binomial regression. *Genome Biology* **20**, 296 (2019).

67. Dobin, A. *et al.* STAR: ultrafast universal RNA-seq aligner. *Bioinformatics* **29**, 15–21 (2012).

68. Mueller, L. A., Zhang, P. & Rhee, S. Y. AraCyc: a biochemical pathway database for Arabidopsis. *Plant Physiol* **132**, 453–460 (2003).

69. Kim, E.-J. *et al.* Plant U-Box40 Mediates Degradation of the Brassinosteroid-Responsive Transcription Factor BZR1 in Arabidopsis Roots. *Plant Cell* **31**, 791–808 (2019).

70. Zhang, X., Henriques, R., Lin, S.-S., Niu, Q.-W. & Chua, N.-H. Agrobacterium-mediated transformation of *Arabidopsis thaliana* using the floral dip method. *Nat. Prot.* **1**, 641–646 (2006).

71. Martin, T., Wöhner, R. V., Hummel, S., Willmitzer, L. & Frommer, W. B. The GUS reporter system as a tool to study plant gene expression. in *GUS protocols: using the GUS gene as a reporter of gene expression* (ed. Gallagher, S. R.) 23–43 (Academic Press, 1992).

72. Lemoine, F. *et al.* NGPhylogeny.fr: new generation phylogenetic services for non-specialists. *Nucleic Acids Research* **47**, W260–W265 (2019).

73. Liu, Z. *et al.* Global dynamic molecular profiling of stomatal lineage cell development by single-cell RNA sequencing. *Molecular Plant* **13**, 1178–1193 (2020).

74. Wang, Y., Huan, Q., Chu, X., Li, K. & Qian, W. Single-cell transcriptome analyses recapitulate the cellular and developmental responses to abiotic stresses in rice. *bioRxiv* 2020.01.30.926329 (2020) doi:10.1101/2020.01.30.926329.

75. Truernit, E., Bauby, H., Belcram, K., Barthélémy, J. & Palauqui, J.-C. OCTOPUS, a polarly localised membrane-associated protein, regulates phloem differentiation entry in *Arabidopsis thaliana*. *Development* **139**, 1306 (2012).

76. Depuydt, S. *et al.* Suppression of *Arabidopsis* protophloem differentiation and root meristem growth by CLE45 requires the receptor-like kinase BAM3. *Proc Natl Acad Sci U S A* **110**, 7074–7079 (2013).

672 77. Hardtke, C. S. & Berleth, T. The *Arabidopsis* gene MONOPTEROS encodes a transcription factor
673 mediating embryo axis formation and vascular development. *EMBO J* **17**, 1405–1411 (1998).

674 78. Smit, M. E. *et al.* A PXY-mediated transcriptional network integrates signaling mechanisms to control
675 vascular development in Arabidopsis. *Plant Cell* **32**, 319 (2020).

676 79. Lee, K.-H., Utku, A., Qi, L. & Wang, H. The α-Aurora Kinases Function in Vascular Development in
677 *Arabidopsis*. *Plant and Cell Physiology* **60**, 188–201 (2018).

678 80. Koroleva, O. A. & Cramer, R. Single-cell proteomic analysis of glucosinolate-rich S-cells in *Arabidopsis*
679 *thaliana*. *Methods* **54**, 413–423 (2011).

680 81. Nintemann, S. J. *et al.* Localization of the glucosinolate biosynthetic enzymes reveals distinct spatial
681 patterns for the biosynthesis of indole and aliphatic glucosinolates. *Physiol. Plant.* **163**, 138–154 (2018).

682 82. Li, J., Kristiansen, K. A., Hansen, B. G. & Halkier, B. A. Cellular and subcellular localization of flavin-
683 monooxygenases involved in glucosinolate biosynthesis. *J. Exp. Bot.* **62**, 1337–1346 (2010).

684 83. Hunziker, P., Halkier, B. A. & Schulz, A. *Arabidopsis* glucosinolate storage cells transform into phloem
685 fibres at late stages of development. *J. Exp. Bot.* **70**, 4305–4317 (2019).

686 84. Gigolashvili, T. *et al.* The transcription factor HIG1/MYB51 regulates indolic glucosinolate biosynthesis
687 in *Arabidopsis thaliana*. *Plant J.* **50**, 886–901 (2007).

688 85. Aubry, S., Smith-Unna, R. D., Boursnell, C. M., Kopriva, S. & Hibberd, J. M. Transcript residency on
689 ribosomes reveals a key role for the *Arabidopsis thaliana* bundle sheath in sulfur and glucosinolate
690 metabolism. *The Plant Journal* **78**, 659–673 (2014).

691

692

ACKNOWLEDGEMENTS

We thank Colin P. S. Kruse (Los Alamos National Laboratory, USA) for constructive comments on the metabolic pathway activity analysis, Thomas Hartwig (WBF lab) for cDNA library preparation for bulk RNA-sequencing, Sebastian Hänsch for assistance with confocal microscope imaging (Center for Advanced Imaging, HHU, Germany), and Xiaoqing Qu (Bio-Protocol, China) for helping with the generation of pSWEET13:SWEET13-YFP construct. This research was supported by the National Science Foundation (SECRETome Project: Systematic Evaluation of CellulaR ExporT from plant cells, IOS-1546879), Deutsche Forschungsgemeinschaft (DFG, German Research Foundation) under Germany´s Excellence Strategy – EXC-2048/1 – project ID 390686111 and SFB 1208 – Project-ID 267205415, as well as the Alexander von Humboldt Professorship to WBF.

AUTHOR INFORMATION

Affiliations

Institute for Molecular Physiology and Cluster of Excellence on Plant Sciences (CEPLAS), Heinrich-Heine-University Düsseldorf, Düsseldorf 40225, Germany

Ji-Yun Kim, Diana Weidauer, Margaret Bezrutczyk, Manuel Miras, Michael M. Wudick, Nora Zöllner & Wolf B. Frommer

Center for Plant Molecular Biology, University of Tübingen, Auf der Morgenstelle 32, 72076 Tübingen, Germany

Efthymia Symeonidi, Tom Denyer & Marja C.P Timmermans

Institute for Computer Science and Department of Biology, Heinrich-Heine-University Düsseldorf, Düsseldorf 40225, Germany

Tin Yau Pang & Martin Lercher

Institute of Transformative Bio-Molecules (WPI-ITbM), Nagoya University, Chikusa, Nagoya 464-8601, Japan

Wolf B. Frommer

Department of Plant Biology, School of Integrative Biology, University of Illinois at Urbana-Champaign, Urbana, Illinois 61801, U.S.A

Li-Qing Chen

Author contributions

J.Y.K. and W.B.F. conceived and supervised the projects. J.Y.K. and T.D. generated the scRNA-seq libraries. E.S. and J.Y.K. performed bioinformatics analyses. J.Y.K., M.B., M.M., M.M.W. and W.B.F. analyzed clusters, J.Y.K., D.W., N.Z., and L.Q.C. generated and analyzed reporter lines. T.Y.P. performed metabolic pathway activity analyses in consultation with M.J.L., J.Y.K. and W.B.F. wrote the manuscript. All authors discussed the results and commented on the manuscript.

ETHIC DECLARATIONS

Competing interests

The authors declare no competing interests.

SUPPLEMENTARY INFORMATION

Supplementary Text

Supplementary Figs 1-13, Supplementary Tables 1-15, Supplementary Video 1

738 **Correspondence and requests for materials** should be addressed to Ji-Yun Kim (email: jiyun.kim@hhu.de).

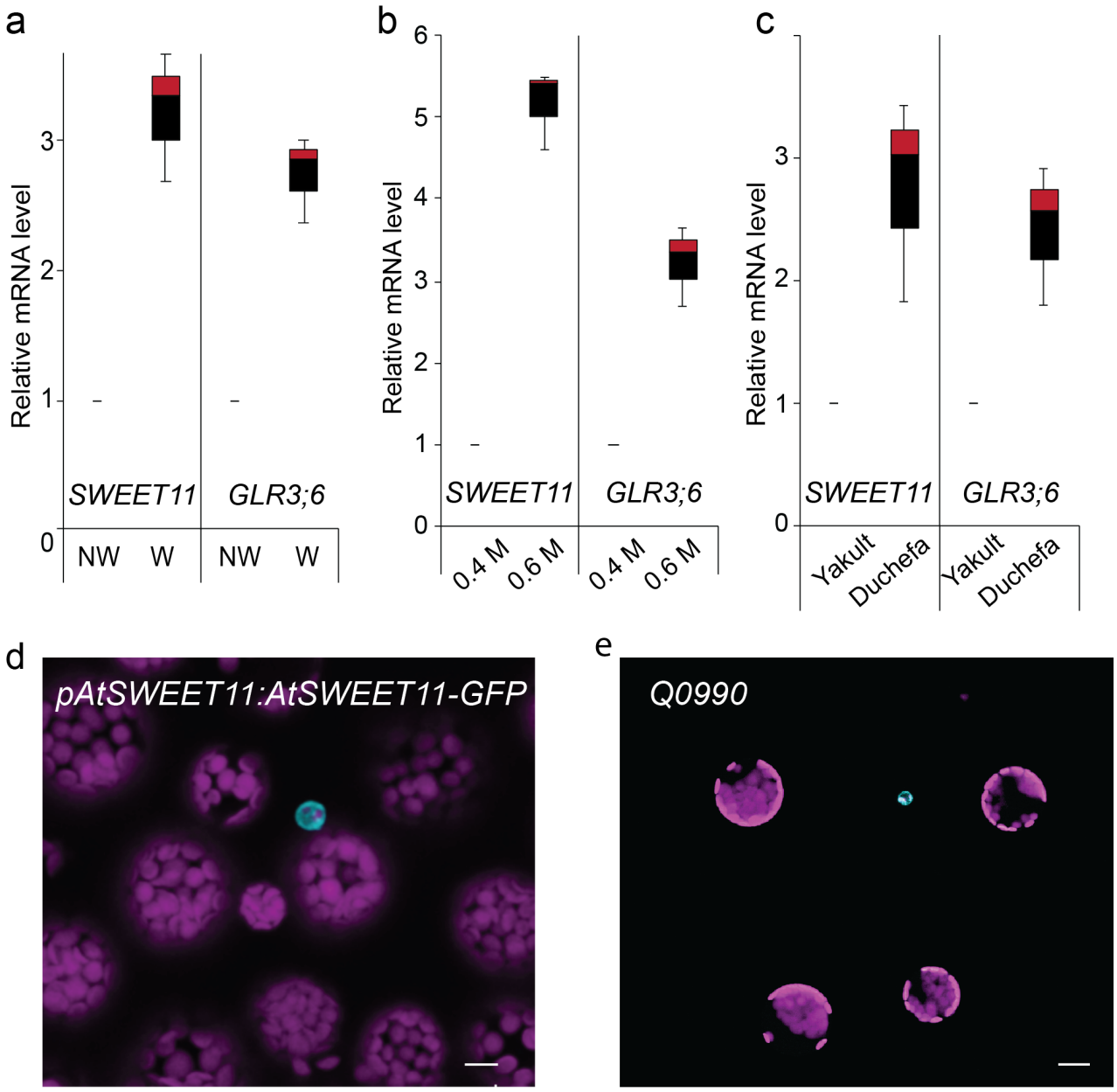

739

740 **Fig. 1: Strategies to enrich vascular protoplasts**

741 **a-c,** Box plot representation of the RT-qPCR analysis results showing the relative transcript level of the
742 marker for the phloem parenchyma, *SWEET11*, and the marker for xylem parenchyma, *GLR3;6*. *UBQ10* was
743 used as an internal control for normalization. The abaxial epidermis was removed from leaves harvested from
744 6-weeks-old plants grown under short day conditions and was treated as indicated. The data shown are from
745 a single experiment with three technical replicates (mean ± SE, n = 3). **a,** Leaves from which the abaxial
746 epidermis had been stripped were either cut on each side of the main vein before enzymatic digestion of the

747 cell wall (wounded, W) or directly placed in the digesting enzyme solution (nonwounded, NW). **b,** Leaves
748 from which the abaxial epidermis had been stripped were cut on each side of the main vein and incubated in
749 the enzyme solution containing 0.4 M or 0.6 M mannitol. **c,** Protoplasts isolated from leaf sample prepared
750 as in **b** were incubated in an enzyme solution composed of cell wall degrading enzymes (cellulase Onozuka
751 R-10, macerozyme R-10) obtained from Yakult (Tokyo) and Duchefa (Haarlem). **d,** GFP fluorescence (cyan)
752 marking phloem parenchyma cells in leaf protoplasts. Protoplasts were isolated from 6-week-old
753 *pAtSWEET11:AtSWEET11-GFP* plants expressing a phloem parenchyma cell-specific marker. Magenta,
754 chlorophyll autofluorescence. Scale bar: 10 μm. e, GFP fluorescence (cyan) marking procambium cells in
755 leaf protoplasts. Protoplasts were isolated from 6-week-old *Q0990* plants expressing a procambium cell-
756 specific marker. Magenta, chlorophyll autofluorescence. Scale bar: 20 μm.

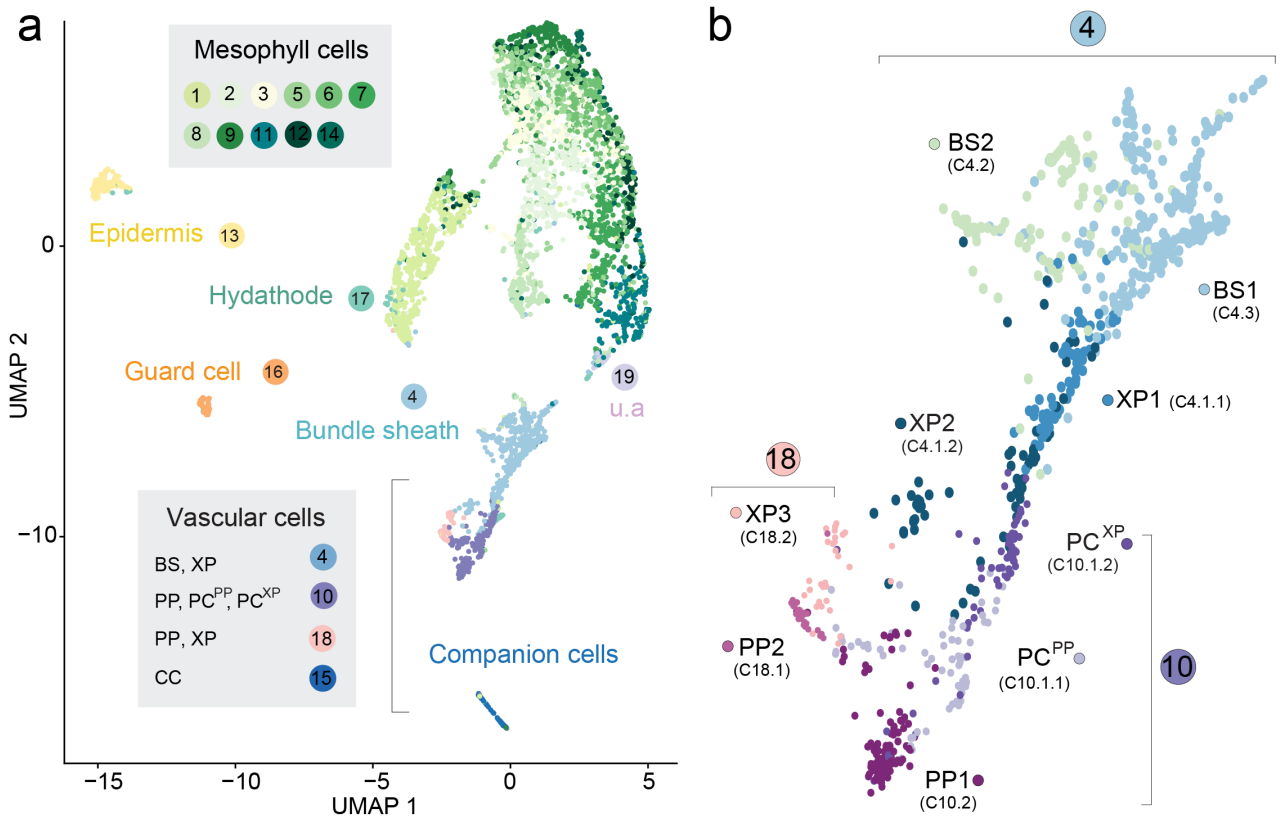

Fig. 2: Assignment of cellular identity to clusters

a, UMAP dimensional reduction projection of 5,230 Arabidopsis leaf cells. Cells were grouped into 19 distinct clusters using Seurat[65]. The cluster number is shown and colored based on the colors assigned to each cell type (u.a. – unassigned, i.e., cluster could not be assigned to a known cell type). Each dot indicates individual cells colored according to the cell type assigned. **b,** Magnification of subclusters C4, C18, and C10. Different colors indicate distinct cell identities. PC: procambium, BS: bundle sheath, XP: xylem parenchyma, PP: phloem parenchyma, PC^{XP}: procambium cells with features relating to xylem differentiation, PC^{PP}: procambium cells with features relating to phloem differentiation.

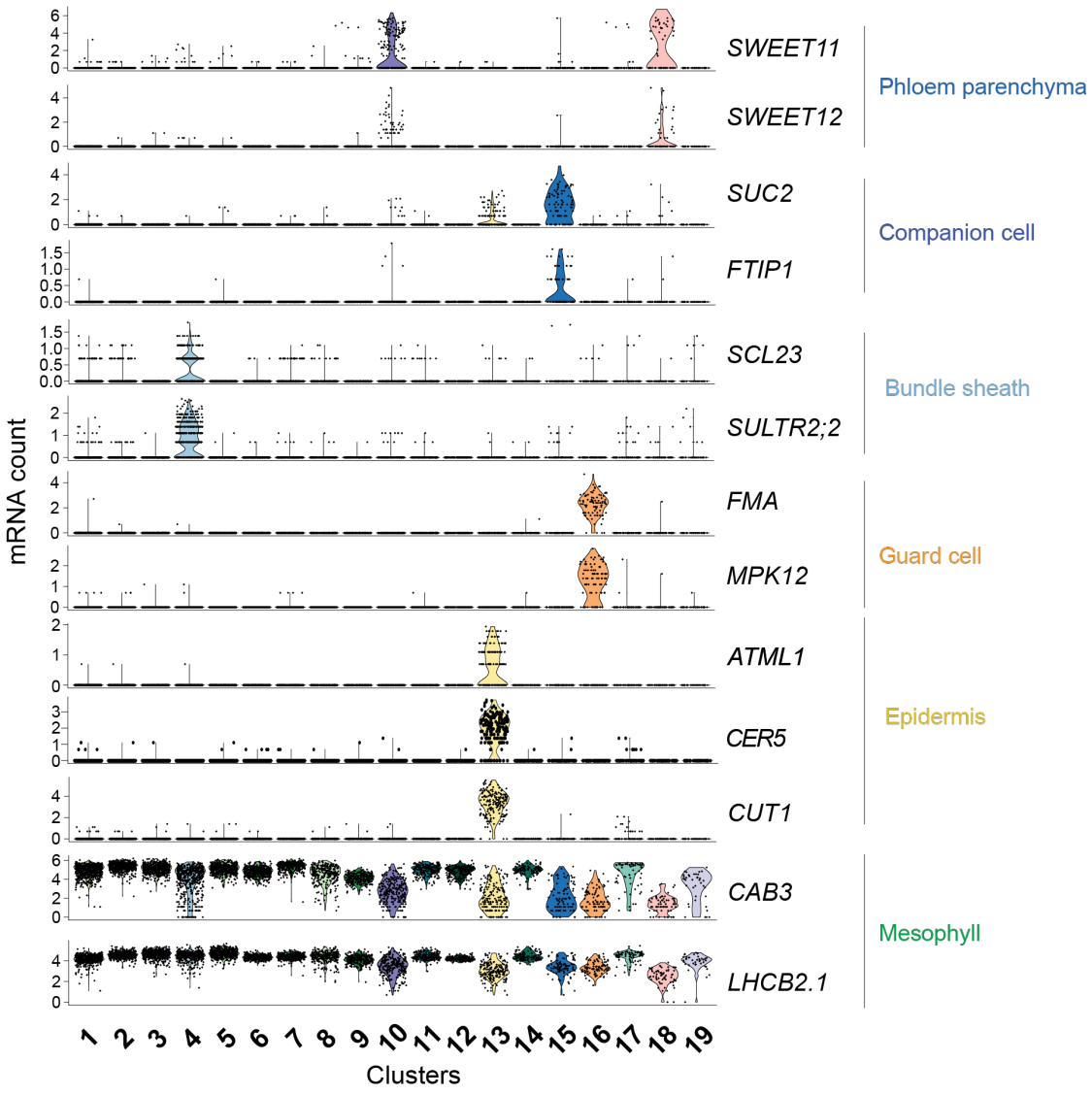

Fig. 3: mRNA levels of marker genes in clusters used to assign cell types

Violin plots showing transcript enrichment of known cell type-specific marker genes across clusters. Clusters are indicated on the x-axis. The name of the cell type assigned to each cluster is indicated on the right side of the violin plots.

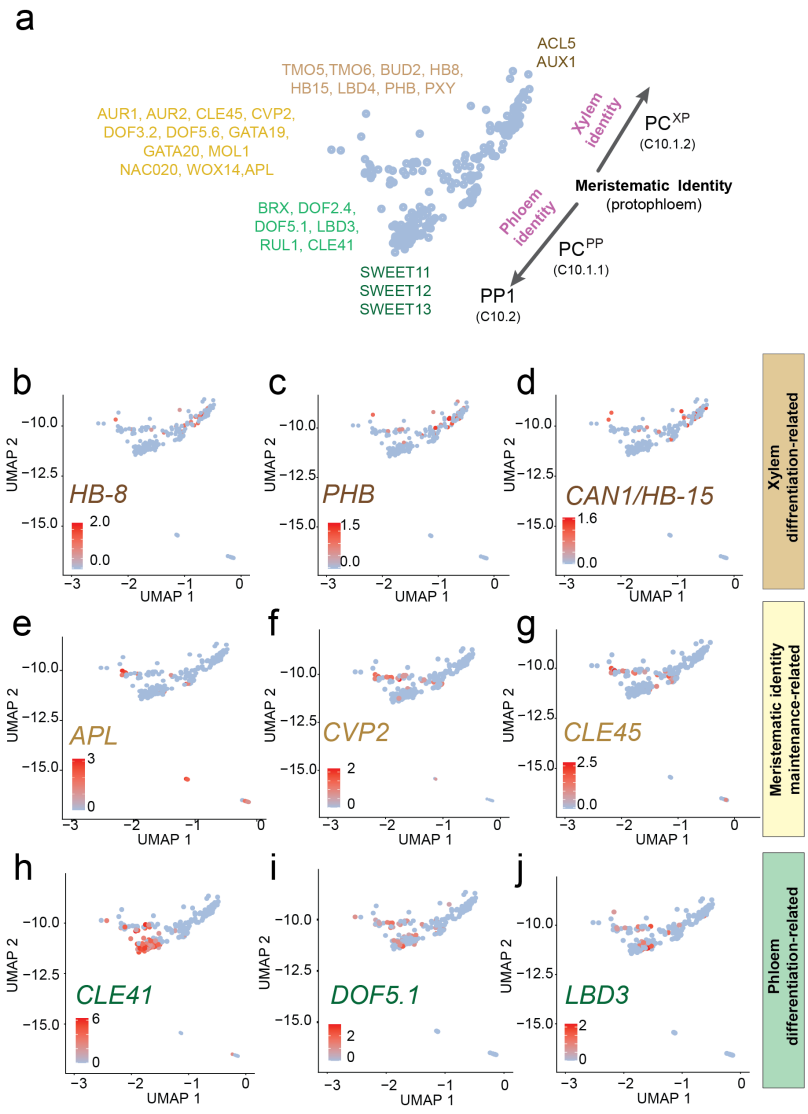

773

774 **Fig. 4: Identification of the procambium cell cluster with distinct procambium cell identities.**

775 **a,** Schematics representing subpopulations of Cluster 10. Genes enriched in the subpopulations are indicated.

776 **b-c,** UMAP showing enrichment of transcripts of genes related to xylem differentiation. **e-g,** UMAP showing

777 enrichment of transcripts of genes related to maintenance of protophloem pluripotency and differentiation.

778 **h-j,** UMAP showing the distribution transcripts related to phloem differentiation.

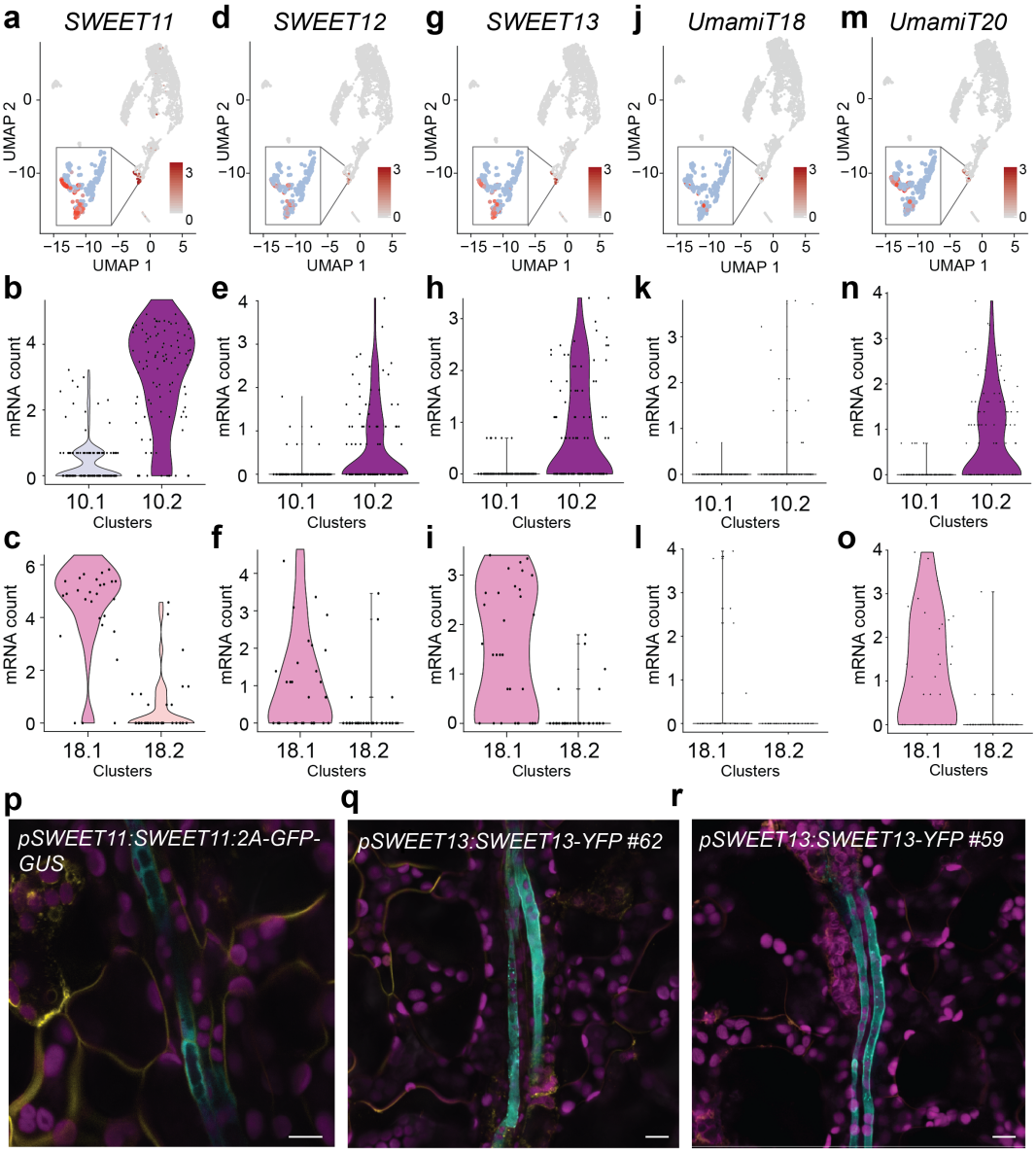

779

780 **Fig. 5: Three SWEET sucrose transporters and UmamiT amino acid transporters mark the phloem**

781 **parenchyma cluster**

782 **a-o,** UMAP and violin plots of C10 and C18 subclusters showing enrichment of *SWEET11*(**a-c**), *SWEET12*(**d-**

783 **f**), *SWEET13*(**g-i**), *UmamiT18/SIAR1*(**j-l**), and *UmamiT20*(**m-o**) transcripts in phloem parenchyma clusters.

784 Subcluster 10.1 corresponds to PC, 18.2 to XP3, and 10.2 and 18.1 to PP. Inset show magnification of C10

785 and C18. **p-r**, Confocal microscopy images of *SWEET11:SWEET11-2A-GFP-GUS* and (**p**),

786 *pSWEET13:SWEET13-YFP*(**q,r**) transgenic plants showing specific GFP(**p**) or YFP(**q,r**) signal in the PP.

Magenta, chlorophyll autofluorescence. Yellow, FM4-64FX. Cyan GFP fluorescence (**p**) or YFP fluorescence(**q,r**). Scale bars: 10 μm.

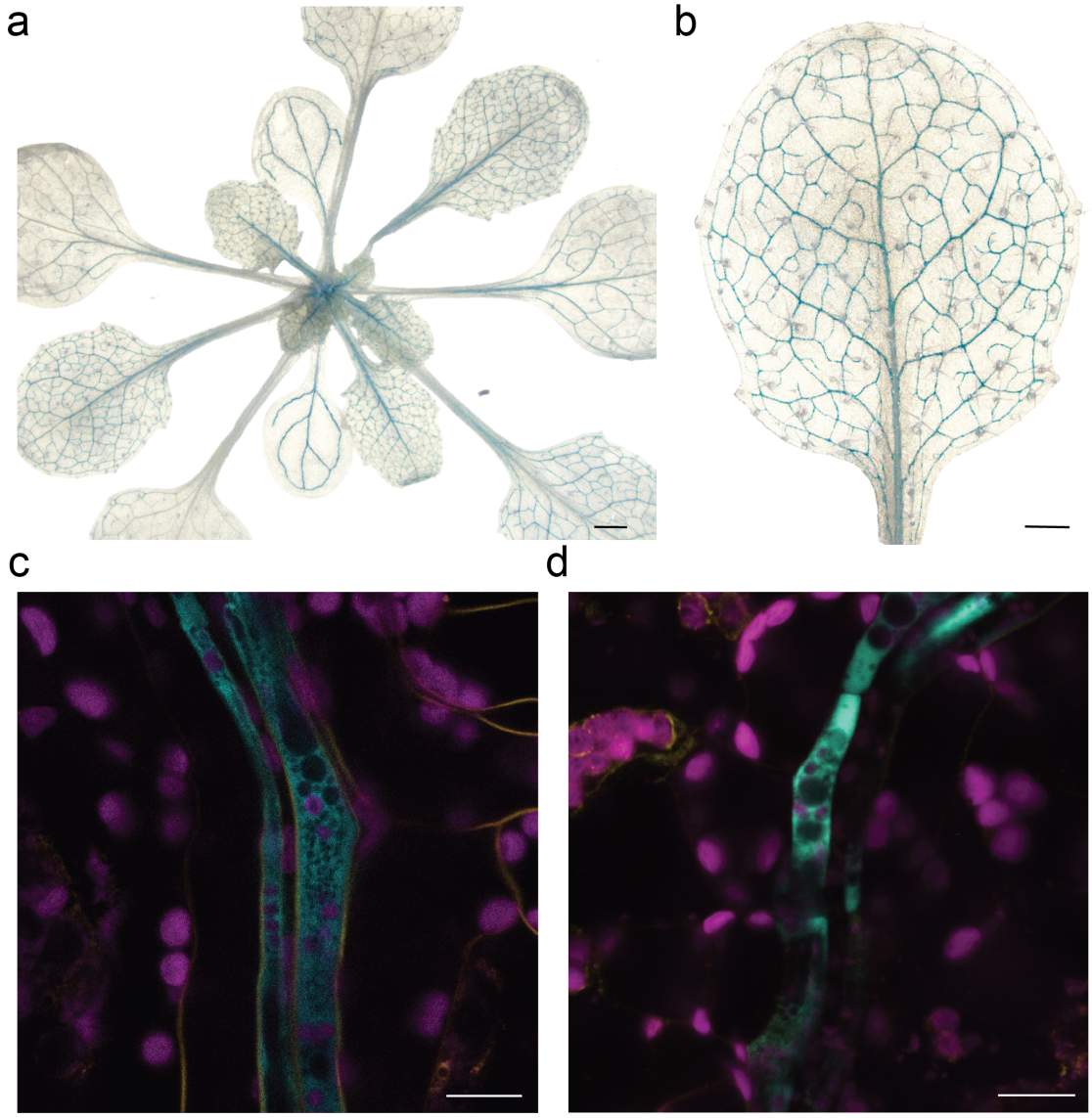

Fig. 6: Reporter gene analysis of *pbZIP9:GFP-GUS* plants.

a,b, GUS stained transgenic plants expressing the transcriptional *pbZIP9:GFP-GUS* reporter construct show GUS activity in the leaf vasculature. Scale bars: 1 mm (**a**) and 0.5 mm (**b**).

796 **c,d** Confocal microscopy images of *pbZIP9:GFP-GUS* reporter lines showing GFP signal specific in the
797 phloem parenchyma cells. Magenta, chlorophyll autofluorescence. Yellow, FM4-64FX, Cyan, GFP
798 fluorescence. Scale bar: 10 μm.

799

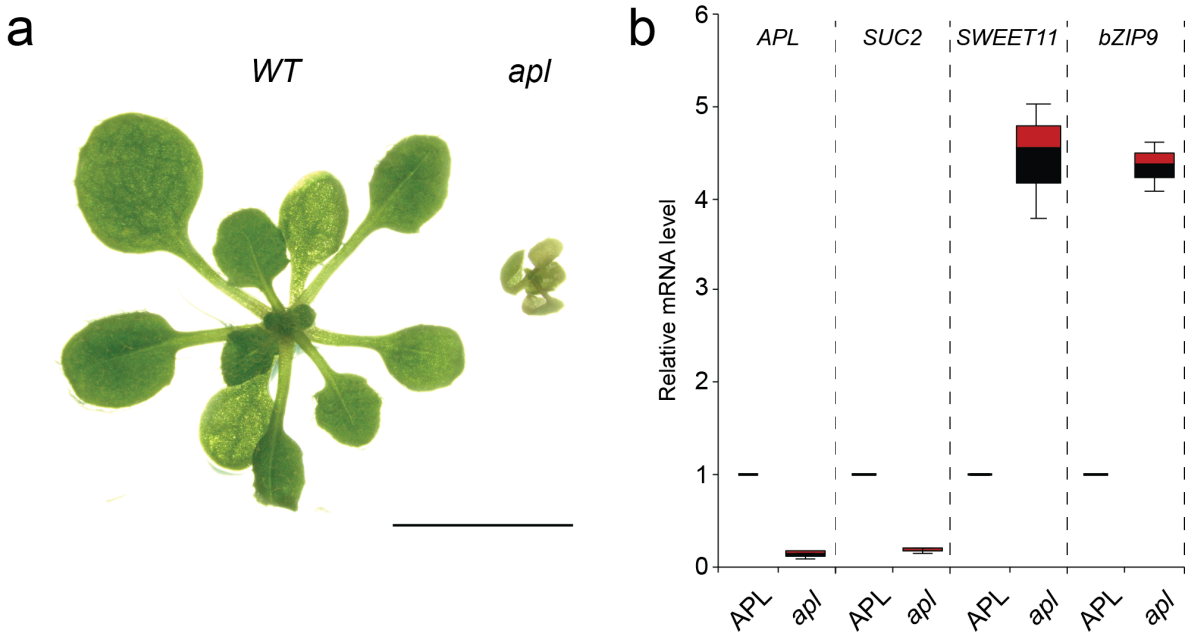

800

801 Figure 7. Distinct PP and CC marker gene expression in the *apl* mutant

802 a, Morphology of *apl* mutant (right) grown on LD conditions for 2 weeks. WT plant grown under the same

803 condition is shown on the left side. Scale bar: 1 cm

804 b. RT-qPCR analysis of CC- marker gene (*SUC2*), and PP- marker genes (*SWEET11* and *bZIP9*). Segregating

805 seeds from heterozygous parents were plated on MS for 2 weeks. The first and second leaves from plants

806 homozygous for the APL mutation (*apl*) and heterozygous for the mutation or WT (APL) were collected for

807 RNA extraction and RT-qPCR. Three independent replicates showed similar results and a representative

808 experiment with three technical replicates are shown (mean ± SE, n = 3).

809

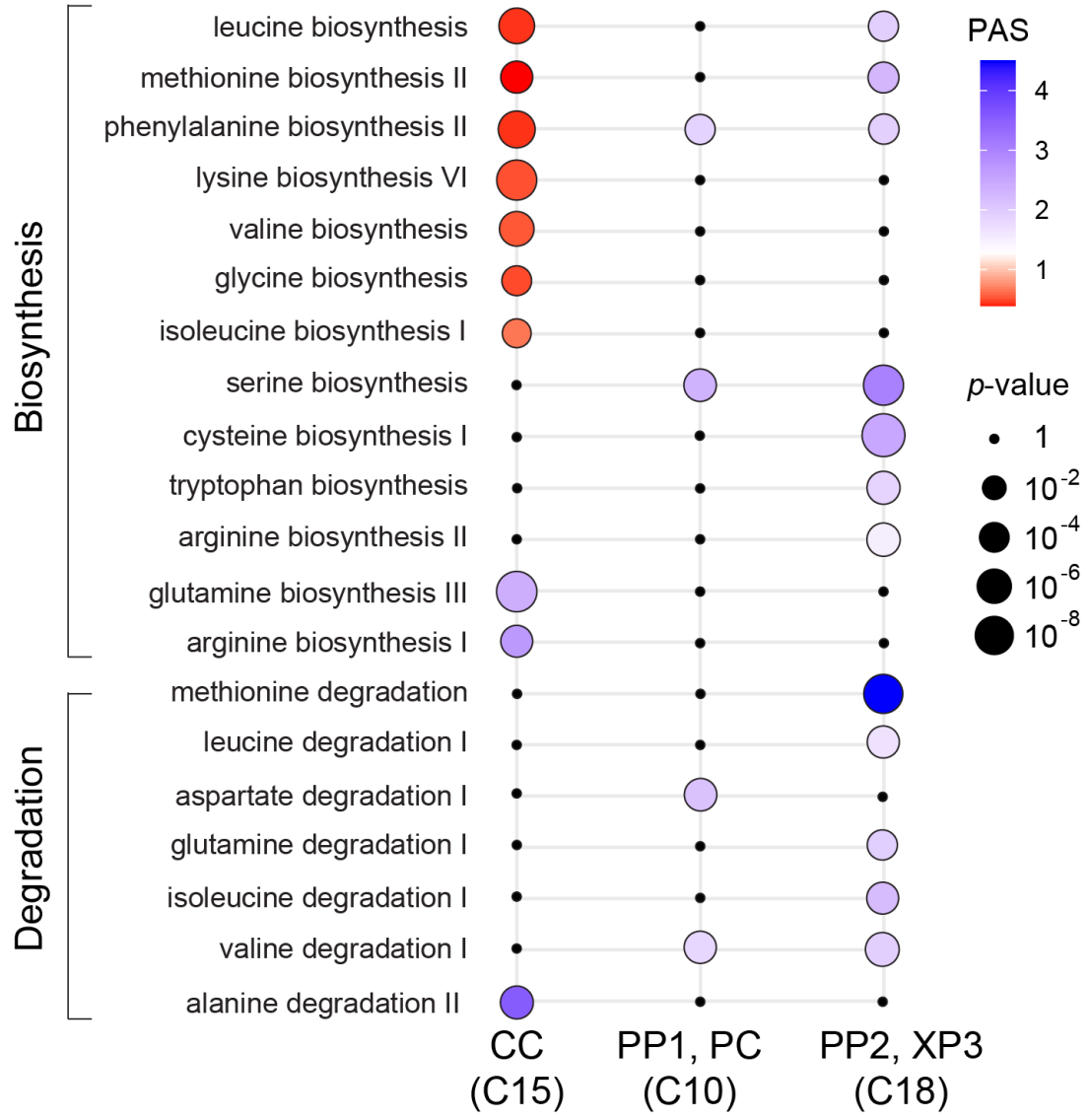

Fig. 8. Amino acid biosynthesis and degradation pathways are differentially represented in the CC PP, PC, and XP3 cells.

Metabolic pathway activities of amino acid biosynthesis and degradation pathways in Clusters 15, 10, and 18. Statistical significance is represented as differences in dot size. Statistically insignificant values are shown as black dots (random permutation test, p >0.05). Colors represent the pathway activity score (PAS); a score <1 (red) reflects a lower than average activity of the pathway in the given cell type, a score >1 (violet) indicates a higher activity. Activities were compared between all clusters in the scRNA-seq dataset.

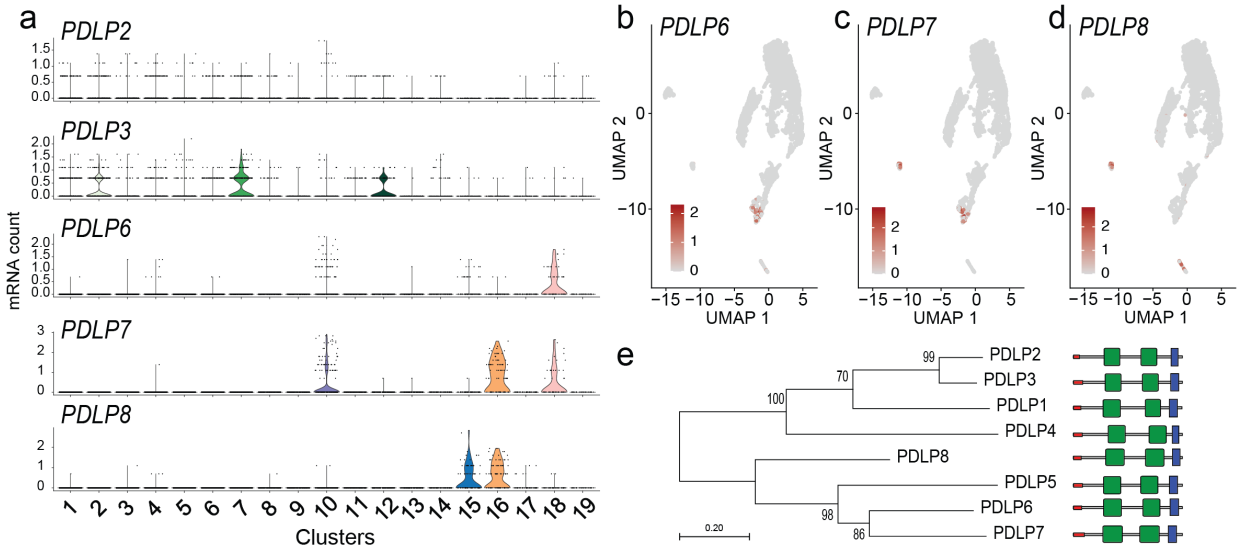

Fig. 9: Transcript enrichment of *PDLP* genes in vascular cell types

a, Violin plot showing transcript enrichment of *PDLP*s. **b-d,** UMAP plot showing the enrichment of *PDLP6* **(b)**, *PDLP7* **(c)** and *PDLP8* **(d)** transcripts in the PP clusters (**b,c**), guard cell cluster (**c,d**), and CC cluster (**d**). **e,** Phylogenetic analysis of PDLPs in Arabidopsis. The phylogenetic tree was generated with the maximum likelihood method implemented in PhyML[72]. Percent support values from 1000 bootstrap samples are shown. Protein motifs predictions are based on the SMART database (http://smart.embl-heidelberg.de). DUF26 domains, transmembrane region and signal peptide are shown in green, blue and red, respectively.

SUPPLEMENTARY TEXT AND DATA

Possible limitations of the scRNA-seq

Despite the advances in scRNA-seq technologies, application to plant cells still faces challenges since the cell walls of plant cells must be removed for the release of individual cells and the penetration of the buffers into cells. Different cell types are likely under different osmotic pressure in the intact plant which might result in breakage if the osmotic conditions are not adequate. Recent studies using Arabidopsis[73], rice[74], as well as maize[57] aerial tissues clearly demonstrate difficulty in capturing vascular cell types reflecting the need for careful strategy development. An unexpected challenge we faced while using loading the cells to the microfluidic chip (10X Genomics) was the sedimentation of mesophyll cells (size of < 50 um). This could also be true for cells from other species but not evident due to the transparent or light color of the cells. However, due to the sedimentation of cells, we observed a 30% loss in the recovery in one of our replicates (Replicate 2). Both libraries showed a high correlation and were therefore used for further analysis. The development of plant cell-specific strategies and compatible buffers will reduce the failure rate and facilitate the application of scRNA-seq analysis in plant tissues from diverse species.

Transcripts enriched in the procambial cluster

Several factors known to be expressed in the phloem precursor cells and play roles in the acquisition of phloem identity such as *ALTERED PHLOEM DEVELOPMENT* (*APL*)[37], a transcription factor known to promote phloem differentiation, and phosphoinositide 5-phosphatases *COTYLEDON VASCULAR PATTERN 2* (*CVP2*) and *CVP2 LIKE 1* (*CVL1*)[34] were detected in the central region of Cluster 10 (C10.1.1) (Fig. 4, Supplementary Fig. 5). *BRX* and *OCTOPUS*[75], important factors involved in protophloem differentiation expressed at different ends of the developing protophloem cells, were also enriched in the nonoverlapping cells in C10.1.1. The protophloem specific *CLAVATA3/EMBRYO SURROUNDING REGION-RELATED 45* (*CLE45*) peptide required for the maintenance of pluripotent phloem cell reservoirs through the interaction with the leucine-rich repeat receptor kinase (LRR-RK), *BARELY ANY MERISTEM 3* (*BAM3*)[35,36], was also detected in subset cells of the procambium cluster. The *CLE45*-enriched cells are in the

854 lower file within the central region (C10.1.1), whereas the *BAM3*-enriched cells are broadly distributed in
855 Cluster 10 with the highest expression in cluster C10.1.1. The distribution of *CLE45* and *BAM3*-expressing
856 cells in our UMAP is reminiscent of the overlapping and nonoverlapping distribution pattern of *CLE45* and
857 *BAM3* in roots[76] suggesting that the mechanism for retaining the plastic identity of the root might also be
858 present in the leaf.

859 Proper control of cell division and proliferation rate is a critical factor for maintaining the meristematic state
860 of the procambium. The auxin response factor MONOPTEROS (MP)[77] plays a role in vascular proliferation
861 by activating of *TARGET OF MONOPTEROS 5* and the auxin and cytokinin responsive DOF family
862 transcription factor *TARGET OF MONOPTEROS 6 (TMO6)*. *TMO6* is further regulated by the receptor
863 kinase PHLOEM INTERCALATED WITH XYLEM and is part of the feed-forward loop involving
864 WUSCHEL HOMEOBOX RELATED 14 (WOX14), TMO6 and LATERAL ORGAN BOUNDARIES
865 DOMAIN 4 (LBD4). This feed-forward loop takes place the boundary of the phloem and procambium cells
866 and influences the distribution of phloem by promoting cell division [78]. We detected *WOX14* transcripts in a
867 few cells at the central region of the procambium cluster. *LBD4* and *TMO6* transcript are present in the
868 boundary of phloem (PP, C10.2) and procambium cell cluster (C10.1.1). Others, including the plant aurora
869 kinases that affect phloem and xylem differentiation negatively through cell division rate control[79], are both
870 enriched in the procambium cell cluster in C10.2.1(Supplementary Fig. 5). Together, we demonstrate that the
871 leaf single-cell sequencing analysis reveals different cell identities within the procambium cluster expressing
872 marker genes identified in various tissues (roots and stems) and show that the spatial distribution of the
873 clusters is well correlated with the distribution of the cell types *in planta*. UMAP plots of additional
874 procambium marker genes in the subpopulations of C10 are shown in Supplementary Fig. 5.

875

876 **Cluster 19 as a candidate for putative S-cell cluster**

877 Glucosinolate-rich cell type (S-cells) are found in floral stems of Arabidopsis but also described as sulfur-
878 rich cells in the phloem parenchyma of the leaf [50]. S cells contain more than tenfold higher sulfur levels, and

879 high levels of glucosinolate compared to the rest of the cells and have been the functional shield of the plant
880 vascular system from herbivores and pathogens. As the S-cells were suggested to be found in the abaxial area
881 of phloem parenchyma in leaves, we questioned whether the S-cells are present in the PP clusters. Markers
882 for S-cells are presently unavailable, therefore, we searched for markers that are known to be absent in S-
883 cells. Proteomic analysis of S-cells has suggested that glucosinolates are not produced in S-cells, as
884 biosynthetic enzymes could not be detected in isolated S-cell extracts . The promoter activities of key
885 enzymes and markers for glucosinolate biosynthesis such as *CYTOCHROME P450 83A1*(*CYP83A1*) and
886 *BRANCHED-CHAIN AMINOTRANSFERASE 4* (*BCAT4*) were not detected in S-cells[81–83]. We detected
887 transcripts of *CYP83A1*, *BCAT4,* as well as other transcripts encoding proteins involved in the synthesis of
888 aliphatic and indolic glucosinolates in the bundle sheath, xylem (C4) and PP/PC/XP (C10, C18) clusters
889 (Supplementary Fig 12). The enrichment of *HIG1* transcription factor which activate promoters of genes
890 involved in glucosinolate biosynthetic genes[84] (Supplementary Tables 4 and 7) also exclude the cells in the
891 PP clusters (C10.2, C18.1) from containing S-cells and suggest the phloem parenchyma, procambium, xylem,
892 and bundle sheath cells as sites for glucosinolate biosynthesis.

893 A unique characteristic of the S-cells is that these cells undergo programmed cell death at the early stages of
894 differentiation. We therefore, searched for cells that could be enriched with the transcripts related to
895 programmed cell death. We identified Cluster 19, a cluster distinct from, but closely spaced to the bundle
896 sheath cells. This cluster was enriched with transcripts related to programmed cell death, hypersensitive
897 response, and defense and immune response (Supplementary Table 13). This cluster also showed high activity
898 scores in insect chewing-induced glucosinolate breakdown pathway (Supplementary Fig. 9b). This result is
899 in line with the primary role of S-cells in releasing toxic compounds through glucosinolate breakdown upon
900 chewing insects induced-mechanical disruption. Although we cannot rule out that these subset cells were
901 clustered based on the stress response from the protoplasting process, they could serve as candidates as
902 putative S-cells.

903

Comprehensive PAS analysis across all cell types

A complete PAS analysis is shown in Supplementary Figure 10.

Highlights from the PAS analysis:

- Glucosinolate biosynthesis activity is high in Cluster 10, Cluster 18, and Cluster 4.
- The pathway activity score of several glucosinolate biosynthesis pathways are low in the GC and CC.
- Mesophyll cells are unlikely sites for glucosinolate biosynthesis nor breakdown.
- The pathway activity scores of glucosinolate breakdown pathways are high in the guard cells.
- Cluster 19 is enriched in glucosinolate breakdown pathway induced by insect chewing.
- Cluster 18 (PP2 and XP3) is enriched with ABA, Ethylene, JA, GA biosynthesis pathways.
- Clusters 10 and 18 are enriched with callose biosynthetic pathways.
- The activity scores of photosynthesis-related pathways are low in non-mesophyll cells (epidermis, CC, guard cell, PP, PC, XP3).

SUPPLEMENTARY TEXT REFERENCES

1. Haritatos, E., Medville, R. & Turgeon, R. Minor vein structure and sugar transport in *Arabidopsis thaliana*. *Planta* **211**, 105–11 (2000).

2. Kang, J. & Dengler, N. Vein pattern development in adult leaves of *Arabidopsis thaliana*. *Int. J. Plant Sci.* **165**, 231–242 (2004).

3. Nguyen, C. T., Kurenda, A., Stolz, S., Chételat, A. & Farmer, E. E. Identification of cell populations necessary for leaf-to-leaf electrical signaling in a wounded plant. *Proc Natl Acad Sci USA* **115**, 10178 (2018).

4. Arun Chinnappa, K. S., Nguyen, T. T. S., Hou, J., Wu, Y. & McCurdy, D. W. Phloem parenchyma transfer cells in *Arabidopsis* - an experimental system to identify transcriptional regulators of wall ingrowth formation. *Front Plant Sci* **4**, 102 (2013).

5. Edwards, J. *et al.* GIGANTEA is a component of a regulatory pathway determining wall ingrowth deposition in phloem parenchyma transfer cells of *Arabidopsis thaliana*. *Plant J.* **63**, 651–661 (2010).

6. Riesmeier, J. W., Willmitzer, L. & Frommer, W. B. Evidence for an essential role of the sucrose transporter in phloem loading and assimilate partitioning. *EMBO J.* **13**, 1–7 (1994).

7. Chen, L. Q. *et al.* Sucrose efflux mediated by SWEET proteins as a key step for phloem transport. *Science* **335**, 207 (2012).

8. Cayla, T., Le Hir, R. & Dinant, S. Live-cell imaging of fluorescently tagged phloem proteins with confocal microscopy. *Methods Mol. Biol.* **2014**, 95–108 (2019).

9. Denyer, T. *et al.* Spatiotemporal developmental trajectories in the *Arabidopsis* root revealed using high-throughput single-cell RNA sequencing. *Dev. Cell* **48**, 840-852.e5 (2019).

10. Ryu, K. H., Huang, L., Kang, H. M. & Schiefelbein, J. Single-cell RNA sequencing resolves molecular relationships among individual plant cells. *Plant Physiol.* **179**, 1444–1456 (2019).

939 11. Zhang, T.-Q., Xu, Z.-G., Shang, G.-D. & Wang, J.-W. A single-cell RNA sequencing profiles the
940 developmental landscape of Arabidopsis root. *Mol Plant* **12**, 648–660 (2019).

941 12. Shulse, C. N. *et al.* High-throughput single-cell transcriptome profiling of plant cell types. *Cell Rep.* **27**,
942 2241-2247.e4 (2019).

943 13. Jean-Baptiste, K. *et al.* Dynamics of Gene Expression in Single Root Cells of Arabidopsis thaliana. *Plant*
944 *Cell* **31**, 993 (2019).

945 14. Birnbaum, K. *et al.* A gene expression map of the *Arabidopsis* root. *Science* **302**, 1956–60 (2003).

946 15. Wu, F.-H. *et al.* Tape-*Arabidopsis* Sandwich - a simpler *Arabidopsis* protoplast isolation method. *Plant*
947 *Meth.* **5**, 16 (2009).

948 16. Radoeva, T., ten Hove, C. A., Saiga, S. & Weijers, D. Molecular characterization of *Arabidopsis*
949 GAL4/UAS enhancer trap lines identifies novel cell-type-specific promoters. *Plant Physiol.* **171**, 1169
950 (2016).

951 17. Satija, R., Farrell, J. A., Gennert, D., Schier, A. F. & Regev, A. Spatial reconstruction of single-cell gene
952 expression data. *Nat. Biotech.* **33**, 495–502 (2015).

953 18. McInnes, L., Healy, J. & Melville, J. UMAP: uniform manifold approximation and projection for
954 dimension reduction. *arXiv* **eprint arXiv:1802.03426**, (2018).

955 19. Sawchuk, M. G., Donner, T. J., Head, P. & Scarpella, E. Unique and overlapping expression patterns
956 among members of photosynthesis-associated nuclear gene families in *Arabidopsis*. *Plant Physiol.* **148**,
957 1908 (2008).

958 20. Endo, M., Shimizu, H., Nohales, M. A., Araki, T. & Kay, S. A. Tissue-specific clocks in *Arabidopsis*
959 show asymmetric coupling. *Nature* **515**, 419–422 (2014).

960 21. Uemoto, K., Araki, T. & Endo, M. Isolation of Arabidopsis palisade and spongy mesophyll cells.
961 *Methods Mol. Biol.* **1830**, 141–148 (2018).

962 22. Takada, S., Takada, N. & Yoshida, A. *ATML1* promotes epidermal cell differentiation in *Arabidopsis*
963 shoots. *Development* **140**, 1919 (2013).

964 23. Bürkle, L. *et al.* Transport of cytokinins mediated by purine transporters of the PUP family expressed in
965 phloem, hydathodes, and pollen of Arabidopsis. *Plant J.* **34**, 13–26 (2003).

966 24. Haritatos, E., Medville, R. & Turgeon, R. Minor vein structure and sugar transport in *Arabidopsis*
967 *thaliana*. *Planta* **211**, 105–11 (2000).

968 25. Endo, A. *et al.* Drought induction of *Arabidopsis* 9-cis-epoxycarotenoid dioxygenase occurs in vascular
969 parenchyma cells. *Plant Physiol* **147**, 1984–1993 (2008).

970 26. Pilot, G. *et al.* Overexpression of GLUTAMINE DUMPER1 leads to hypersecretion of glutamine from
971 hydathodes of Arabidopsis leaves. *Plant Cell* **16**, 1827–40 (2004).

972 27. Okumoto, S. *et al.* High affinity amino acid transporters specifically expressed in xylem parenchyma and
973 developing seeds of Arabidopsis. *Journal of Biological Chemistry* **277**, 45338–45346 (2002).

974 28. Dinkeloo, K., Boyd, S. & Pilot, G. Update on amino acid transporter functions and on possible amino
975 acid sensing mechanisms in plants. *Sem Cell Dev Biol* **74**, 105–113 (2018).

976 29. Madsen, S. R., Olsen, C. E., Nour-Eldin, H. H. & Halkier, B. A. Elucidating the role of transport
977 processes in leaf glucosinolate distribution. *Plant Physiol.* **166**, 1450 (2014).

978 30. Nour-Eldin, H. H. *et al.* NRT/PTR transporters are essential for translocation of glucosinolate defence
979 compounds to seeds. *Nature* **488**, 531–534 (2012).

980 31. Sanchez, P., Nehlin, L. & Greb, T. From thin to thick: major transitions during stem development. *Trends*
981 *Plant Sci* **17**, 113–121 (2012).

982 32. Elo, A., Immanen, J., Nieminen, K. & Helariutta, Y. Stem cell function during plant vascular
983 development. *Sem. Cell Dev. Biol.* **20**, 1097–1106 (2009).

984 33. Baima, S. *et al.* The *Arabidopsis* ATHB-8 HD-zip protein acts as a differentiation-promoting
985 transcription factor of the vascular meristems. *Plant Physiol* **126**, 643–655 (2001).

986 34. Rodriguez-Villalon, A., Gujas, B., van Wijk, R., Munnik, T. & Hardtke, C. S. Primary root protophloem
987 differentiation requires balanced phosphatidylinositol-4,5-biphosphate levels and systemically affects
988 root branching. *Development* **142**, 1437 (2015).

989 35. Gujas, B. *et al.* A reservoir of pluripotent phloem cells safeguards the linear developmental trajectory of
990 protophloem sieve elements. *Curr. Biol.* **30**, 755-766.e4 (2020).

991 36. Rodriguez-Villalon, A. *et al.* Molecular genetic framework for protophloem formation. *Proc Natl Acad*
992 *Sci USA* **111**, 11551 (2014).

993 37. Bonke, M., Thitamadee, S., Mähönen, A. P., Hauser, M.-T. & Helariutta, Y. APL regulates vascular
994 tissue identity in *Arabidopsis*. *Nature* **426**, 181–186 (2003).

995 38. Chen, L. Q. *et al.* Sucrose efflux mediated by SWEET proteins as a key step for phloem transport. *Science*
996 **335**, 207–11 (2012).

997 39. Gottwald, J. R., Krysan, P. J., Young, J. C., Evert, R. F. & Sussman, M. R. Genetic evidence for the *in*
998 *planta* role of phloem-specific plasma membrane sucrose transporters. *Proc Natl Acad Sci USA* **97**,
999 13979 (2000).

1000 40. Ladwig, F. *et al.* Siliques are Red1 from Arabidopsis acts as a bidirectional amino acid transporter that
1001 is crucial for the amino acid homeostasis of siliques. *Plant Physiol.* **158**, 1643–55 (2012).

1002 41. Zhang, L. *et al.* Altered xylem-phloem transfer of amino acids affects metabolism and leads to increased
1003 seed yield and oil content in *Arabidopsis*. *Plant Cell* **22**, 3603–3620 (2010).

1004 42. Schachtman, D. P., Schroeder, J. I., Lucas, W. J., Anderson, J. A. & Gaber, R. F. Expression of an inward-
1005 rectifying potassium channel by the *Arabidopsis* KAT1 cDNA. *Science* **258**, 1654–1658 (1992).

1006 43. Chen, L. Q. *et al.* Sugar transporters for intercellular exchange and nutrition of pathogens. *Nature* **468**,
1007 527–532 (2010).

1008 44. Weichert, A. *et al.* AtPTR4 and AtPTR6 are differentially expressed, tonoplast-localized members of the
1009 peptide transporter/nitrate transporter 1 (PTR/NRT1) family. *Planta* **235**, 311–323 (2012).

1010 45. Mustroph, A. *et al.* Profiling translatomes of discrete cell populations resolves altered cellular priorities
1011 during hypoxia in Arabidopsis. *Proc Natl Acad Sci USA* **106**, 18843–8 (2009).

1012 46. Fischer, W. N., Kwart, M., Hummel, S. & Frommer, W. B. Substrate specificity and expression profile
1013 of amino acid transporters (AAPs) in Arabidopsis. *Journal of Biological Chemistry* **270**, 16315–16320
1014 (1995).

1015 47. Atkins, C. A. Biochemical aspects of assimilate transfers along the phloem path: N-solutes in lupins.
1016 *Austr. J. Plant Physiol.* **27**, 531–537 (2000).

1017 48. Metzler, A. *et al.* Plant histochemistry by correlation peak imaging. *Proc. Natl. Acad. Sci. USA* **92**,
1018 11912–5 (1995).

1019 49. Xiao, Z., Dai, Z. & Locasale, J. W. Metabolic landscape of the tumor microenvironment at single cell
1020 resolution. *Nature Communications* **10**, 3763 (2019).

1021 50. Koroleva, O. A., Gibson, T. M., Cramer, R. & Stain, C. Glucosinolate-accumulating S-cells in
1022 *Arabidopsis* leaves and flower stalks undergo programmed cell death at early stages of differentiation.
1023 *Plant J.* **64**, 456–469 (2010).

1024 51. Maeda, H., Song, W., Sage, T. & DellaPenna, D. Role of callose synthases in transfer cell wall
1025 development in tocopherol deficient Arabidopsis mutants. *Frontiers in Plant Science* **5**, 46 (2014).

1026 52. Lee, J.-Y. *et al.* A plasmodesmata-localized protein mediates crosstalk between cell-to-cell
1027 communication and innate immunity in Arabidopsis. *Plant Cell* **23**, 3353–3373 (2011).

1028 53. Brault, M. L. *et al.* Multiple C2 domains and transmembrane region proteins (MCTPs) tether membranes
1029 at plasmodesmata. *EMBO Rep.* **20**, e47182 (2019).

1030 54. Tanvir, Z. Expression domain analysis of four members of the plasmodesmata-localized protein family
1031 in Arabidopsis. (University of Delaware, 2016).

1032 55. Liu, L. *et al.* FTIP1 Is an essential regulator required for florigen transport. *PLoS Biol.* **10**, e1001313
1033 (2012).

1034 56. Bel, A. J. E. van & Knoblauch, M. Sieve element and companion cell: the story of the comatose patient
1035 and the hyperactive nurse. *Funct. Plant Biol.* **27**, 477–487 (2000).

1036 57. Bezrutczyk, M. *et al.* Phloem loading via the abaxial bundle sheath cells in maize leaves. *Nat. Plants*
1037 **submitted**,.

1038 58. Kühn, C., Franceschi, V. R., Schulz, A., Lemoine, R. & Frommer, W. B. Macromolecular trafficking
1039 indicated by localization and turnover of sucrose transporters in enucleate sieve elements. *Science* **275**,
1040 1298–300 (1997).

1041 59. Chen, L. Q. *et al.* A cascade of sequentially expressed sucrose transporters in the seed coat and
1042 endosperm provides nutrition for the *Arabidopsis* embryo. *Plant Cell* **27**, 607 (2015).

1043 60. Fischer, W.-N. *et al.* Amino acid transport in plants. *Trends Plant Sci.* **3**, 188–195 (1998).

1044 61. Kuromori, T., Sugimoto, E. & Shinozaki, K. Intertissue signal transfer of abscisic acid from vascular
1045 cells to guard cells. *Plant Physiol.* **164**, 1587 (2014).

1046 62. Kanno, Y. *et al.* AtSWEET13 and AtSWEET14 regulate gibberellin-mediated physiological processes.
1047 *Nat. Comm.* **7**, 13245 (2016).

1048 63. Ye, Z.-W. *et al.* Arabidopsis acyl-CoA-binding protein ACBP6 localizes in the phloem and affects
1049 jasmonate composition. *Plant Mol. Biol.* **92**, 717–730 (2016).

1050 64. Nguyen, C. T., Martinoia, E. & Farmer, E. E. Emerging jasmonate transporters. *Mol Plant* **10**, 659–661
1051 (2017).

1052 65. Butler, A., Hoffman, P., Smibert, P., Papalexi, E. & Satija, R. Integrating single-cell transcriptomic data
1053 across different conditions, technologies, and species. *Nat Biotech* **36**, 411–420 (2018).

66. Hafemeister, C. & Satija, R. Normalization and variance stabilization of single-cell RNA-seq data using regularized negative binomial regression. *Genome Biology* **20**, 296 (2019).

67. Dobin, A. *et al.* STAR: ultrafast universal RNA-seq aligner. *Bioinformatics* **29**, 15–21 (2012).

68. Mueller, L. A., Zhang, P. & Rhee, S. Y. AraCyc: a biochemical pathway database for Arabidopsis. *Plant Physiol* **132**, 453–460 (2003).

69. Kim, E.-J. *et al.* Plant U-Box40 Mediates Degradation of the Brassinosteroid-Responsive Transcription Factor BZR1 in Arabidopsis Roots. *Plant Cell* **31**, 791–808 (2019).

70. Zhang, X., Henriques, R., Lin, S.-S., Niu, Q.-W. & Chua, N.-H. Agrobacterium-mediated transformation of *Arabidopsis thaliana* using the floral dip method. *Nat. Prot.* **1**, 641–646 (2006).

71. Martin, T., Wöhner, R. V., Hummel, S., Willmitzer, L. & Frommer, W. B. The GUS reporter system as a tool to study plant gene expression. in *GUS protocols: using the GUS gene as a reporter of gene expression* (ed. Gallagher, S. R.) 23–43 (Academic Press, 1992).

72. Lemoine, F. *et al.* NGPhylogeny.fr: new generation phylogenetic services for non-specialists. *Nucleic Acids Research* **47**, W260–W265 (2019).

73. Liu, Z. *et al.* Global dynamic molecular profiling of stomatal lineage cell development by single-cell RNA sequencing. *Molecular Plant* **13**, 1178–1193 (2020).

74. Wang, Y., Huan, Q., Chu, X., Li, K. & Qian, W. Single-cell transcriptome analyses recapitulate the cellular and developmental responses to abiotic stresses in rice. *bioRxiv* 2020.01.30.926329 (2020) doi:10.1101/2020.01.30.926329.

75. Truernit, E., Bauby, H., Belcram, K., Barthélémy, J. & Palauqui, J.-C. OCTOPUS, a polarly localised membrane-associated protein, regulates phloem differentiation entry in *Arabidopsis thaliana*. *Development* **139**, 1306 (2012).

76. Depuydt, S. *et al.* Suppression of *Arabidopsis* protophloem differentiation and root meristem growth by CLE45 requires the receptor-like kinase BAM3. *Proc Natl Acad Sci U S A* **110**, 7074–7079 (2013).

77. Hardtke, C. S. & Berleth, T. The *Arabidopsis* gene MONOPTEROS encodes a transcription factor mediating embryo axis formation and vascular development. *EMBO J* **17**, 1405–1411 (1998).

78. Smit, M. E. *et al.* A PXY-mediated transcriptional network integrates signaling mechanisms to control vascular development in Arabidopsis. *Plant Cell* **32**, 319 (2020).

79. Lee, K.-H., Utku, A., Qi, L. & Wang, H. The α-Aurora Kinases Function in Vascular Development in *Arabidopsis*. *Plant and Cell Physiology* **60**, 188–201 (2018).

80. Koroleva, O. A. & Cramer, R. Single-cell proteomic analysis of glucosinolate-rich S-cells in *Arabidopsis thaliana*. *Methods* **54**, 413–423 (2011).

81. Nintemann, S. J. *et al.* Localization of the glucosinolate biosynthetic enzymes reveals distinct spatial patterns for the biosynthesis of indole and aliphatic glucosinolates. *Physiol. Plant.* **163**, 138–154 (2018).

82. Li, J., Kristiansen, K. A., Hansen, B. G. & Halkier, B. A. Cellular and subcellular localization of flavin-monooxygenases involved in glucosinolate biosynthesis. *J. Exp. Bot.* **62**, 1337–1346 (2010).

83. Hunziker, P., Halkier, B. A. & Schulz, A. *Arabidopsis* glucosinolate storage cells transform into phloem fibres at late stages of development. *J. Exp. Bot.* **70**, 4305–4317 (2019).

84. Gigolashvili, T. *et al.* The transcription factor HIG1/MYB51 regulates indolic glucosinolate biosynthesis in *Arabidopsis thaliana*. *Plant J.* **50**, 886–901 (2007).

85. Aubry, S., Smith-Unna, R. D., Boursnell, C. M., Kopriva, S. & Hibberd, J. M. Transcript residency on ribosomes reveals a key role for the *Arabidopsis thaliana* bundle sheath in sulfur and glucosinolate metabolism. *The Plant Journal* **78**, 659–673 (2014).

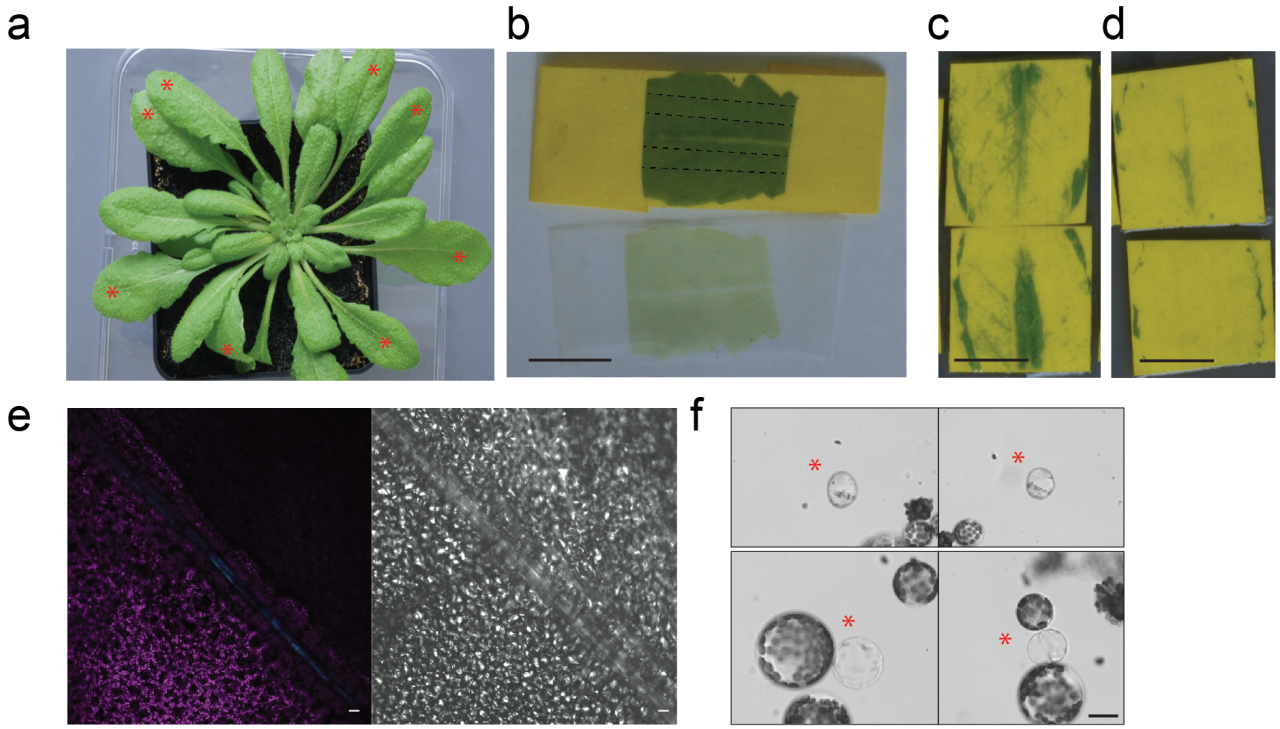

Supplementary Fig. 1: Optimization of vascular protoplast enrichment

a, Six-week-old Arabidopsis plant grown under short-day conditions. Leaves used for protoplasting are marked with red asterisks. **b,** Tape-sandwiched leaf explants were separated and the remaining adaxial side was cut parallel to the main vein. Cutting sites are marked as dotted lines. Scale bar: 1 cm. **c-d,** Tape-separated leaf explants 2 hours after enzyme digest. The release of vascular cells is more effective with an enzyme solution in 0.6 M mannitol (**d**), compared to 0.4 M mannitol (**c**) Scale bar: 1 cm. **e,** Detection of procambial cells in the major vein using the procambial marker *Q0990*. Scale bars: 50 µm. **f,** Diversity of leaf protoplasts. Protoplasts lacking chloroplasts are marked with red asterisks. Scale bar: 20 µm

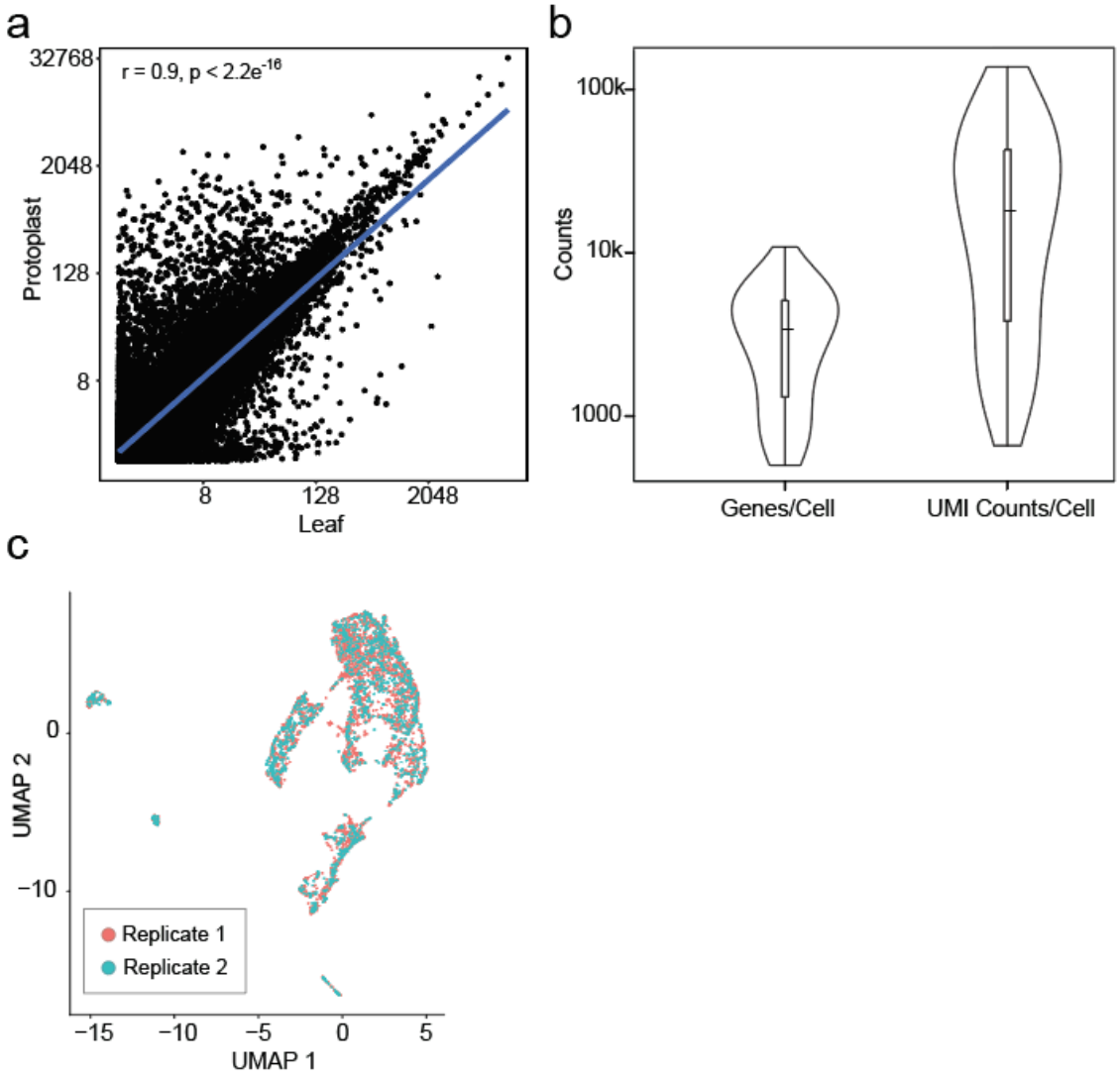

Supplementary Fig. 2: Reliability of Arabidopsis leaf scRNA-seq dataset

a, Correlation of gene expression in bulk leaf (not protoplasted) and bulk protoplasts. r = Pearson´s correlation coefficient. The list of DEGs in bulk RNA-seq of non protoplasted leaf and protoplasted leaf samples are provided in Supplementary Table 1. **b,** Violin plot illustrating the distribution of the number of genes (nFeature RNA) and UMI counts (nCount RNA) detected within a cell. **c,** UMAP plot of 5,230 cell transcriptomes from two biological replicates. Different colors indicate the cells from each replicate.

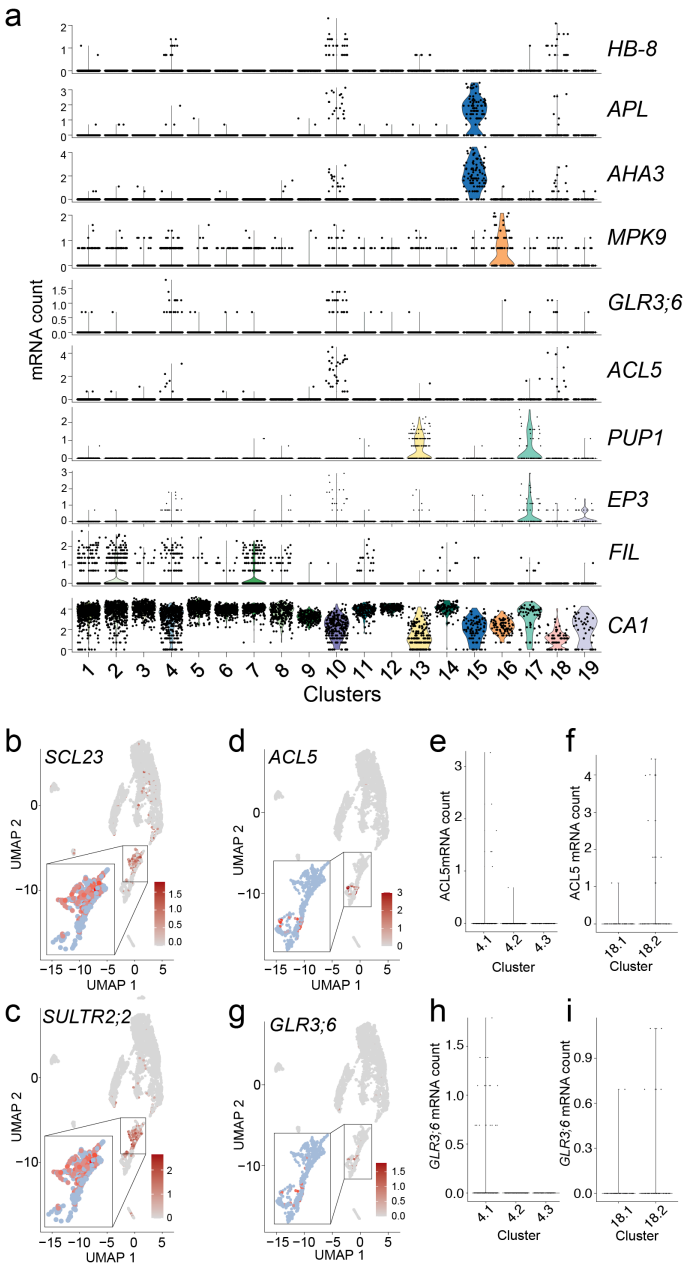

Supplementary Fig. 3: Enrichment of known marker genes for assigning cell types to clusters.

a, Violin plots showing the expression of cell type-specific marker genes across clusters. **b,c,** UMAP plot illustrating the enrichment of bundle sheath (BS) markers, *SCL23* (**b**) and *SULTR2;2* (**c**). Inset shows magnification of Cluster 4. **d-i,** UMAP plot (**d,g**) and violin plots of the subclusters of Cluster 4 (**e,h**) and Cluster 18 (**f,i**) showing enrichment of xylem markers, *ACL5* (**d,e,f**) and *GLR3;6* (**g,h,i**). Magnified views of the boxed region (Clusters 4, 10, and 18) is shown in the insets (**d,g**).

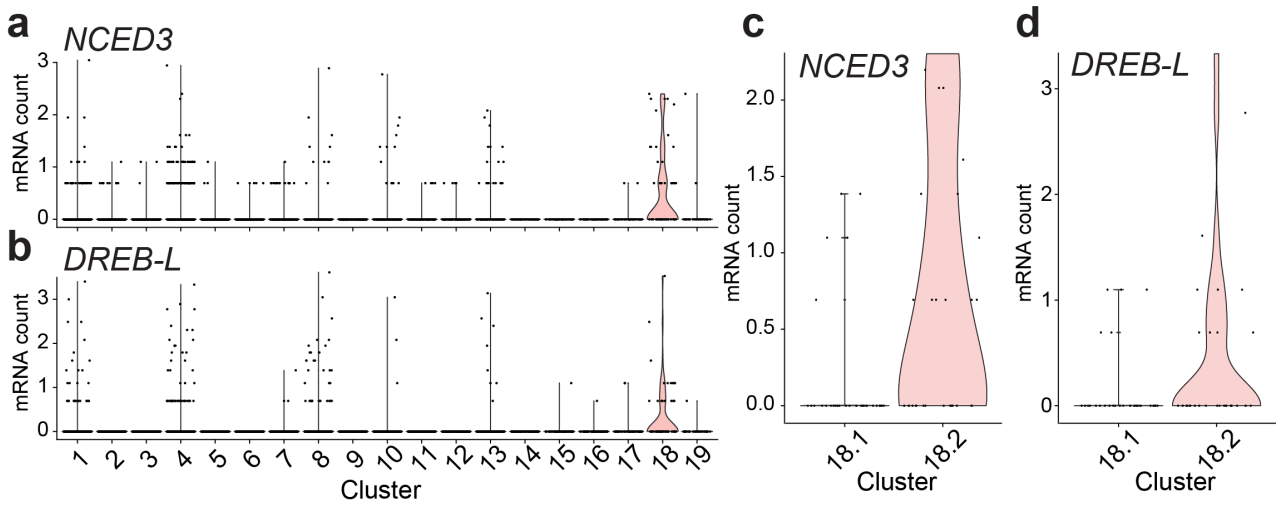

Supplementary Fig. 4: Vascular parenchyma-specific marker genes enriched in Cluster 18 (XP3)

a-d, Violin plots showing the transcript enrichment of *NCED3* (**a,c**) and *DREB-L* (**b,d**) across the main clusters (**a,b**) or subclusters of Cluster 18 (**c,d**).

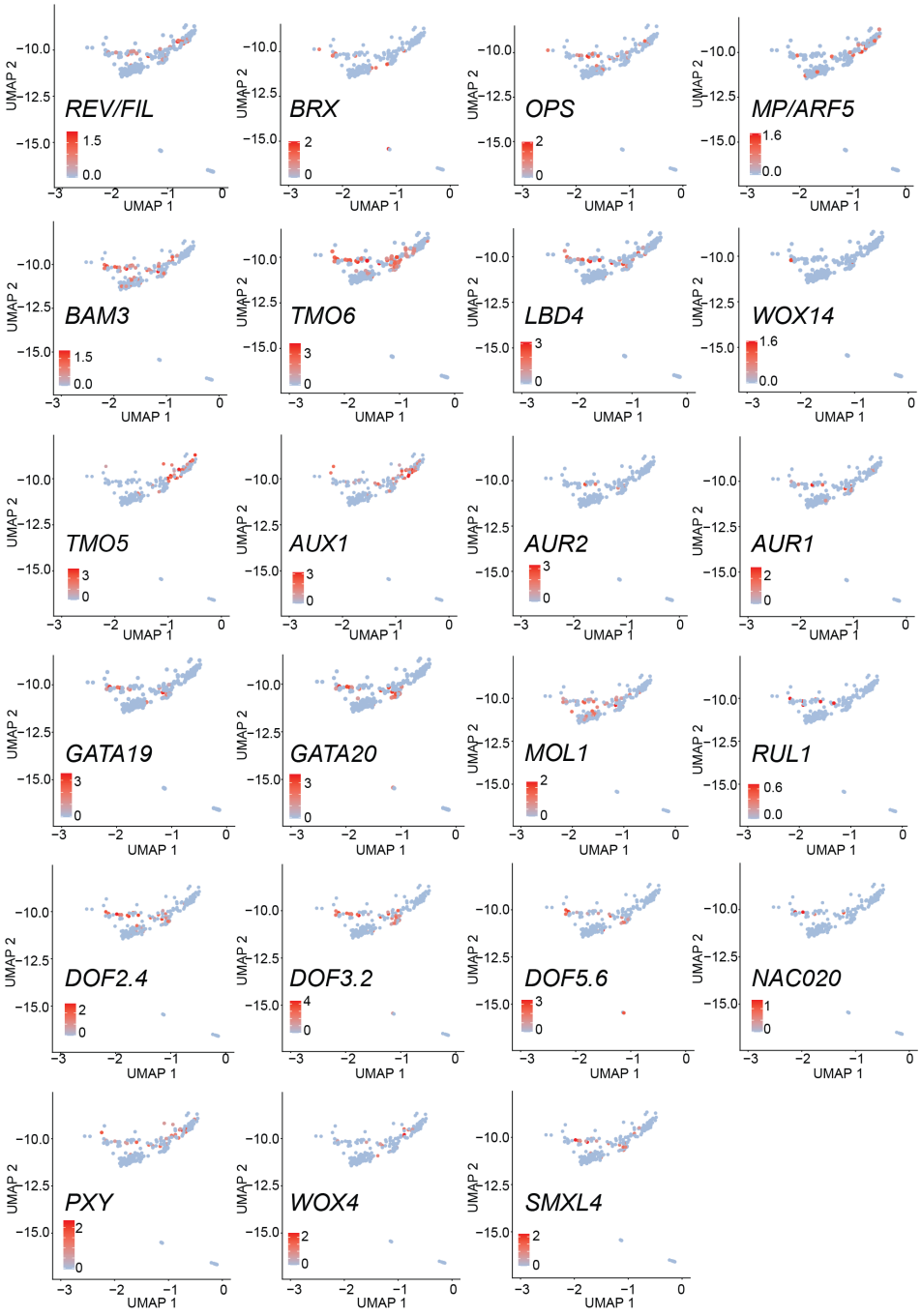

Supplementary Fig. 5: Distinct procambium cell identities in C10 subclusters

UMAP plot showing the distribution of transcripts enriched in C10 subclusters.

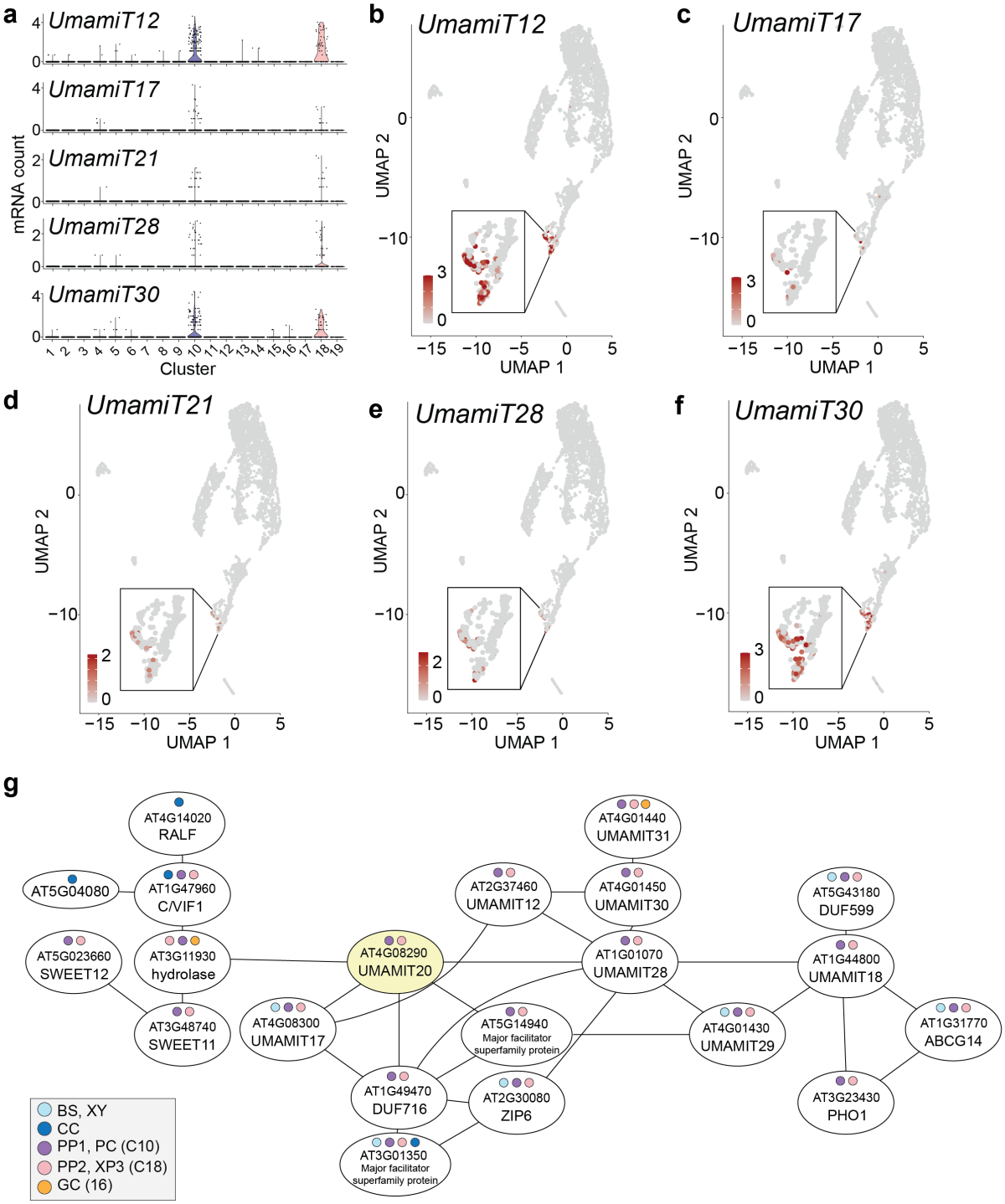

Supplementary Fig. 6: Transcripts of UmamiT amino acid transport family members are enriched in the PP.

a, Violin plots illustrating the transcript enrichment of *UmamiT12*, *UmamiT17, UmamiT21, UmamiT28,* and *UmamiT30*. The cell types assigned to clusters are indicated in **Fig. 2a,b**. **b,** UMAP showing the enrichment

of *UmamiT12* **(b)**, *UmamiT17* **(c)**, *UmamiT21* **(d)**, *UmamiT28* **(e)**, and *UmamiT30* **(f)**. Magnifications of the marked regions are shown in the insets. **g,** Coexpression gene network around *UmamiT20* built from the coexpression database ATTED-II (http://atted.jp). The cell types in which the genes in the network are enriched are marked with colored circles. The colors corresponding to the cell types and clusters are indicated in the bottom left box.

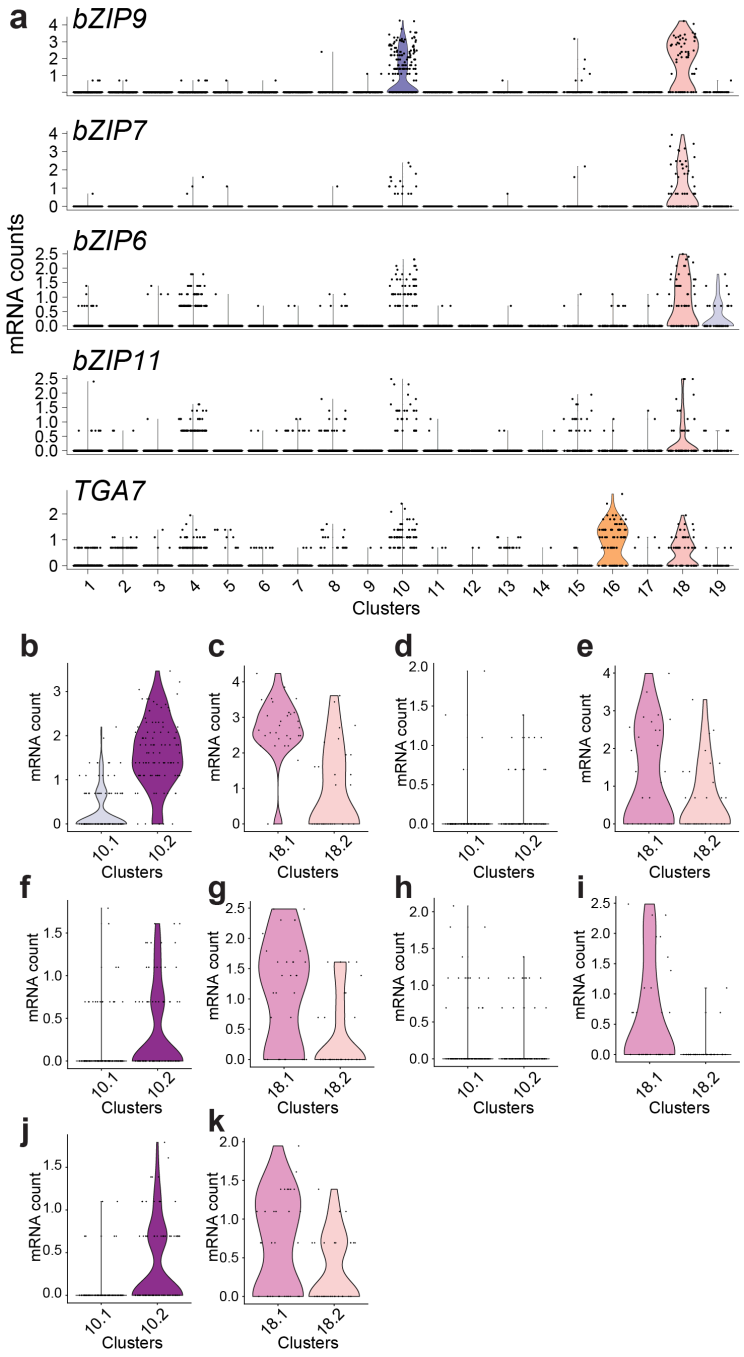

Supplementary Fig. 7: Transcript enrichment of multiple bZIP transcription factors in the PP clusters.

a, Violin plots showing transcript enrichment of five bZIP family members. **b-k,** Violin plots showing transcript enrichment of *bZIP9* (**b,c**), *bZIP7* (**d,e**), *bZIP6* (**f,g**), *bZIP11* (**h,i**), and *TGA7* (**j,k**) in the subclusters of Cluster 10 (**b,d,f,h,j**) and Cluster 18 (**c,e,g,i,k**).

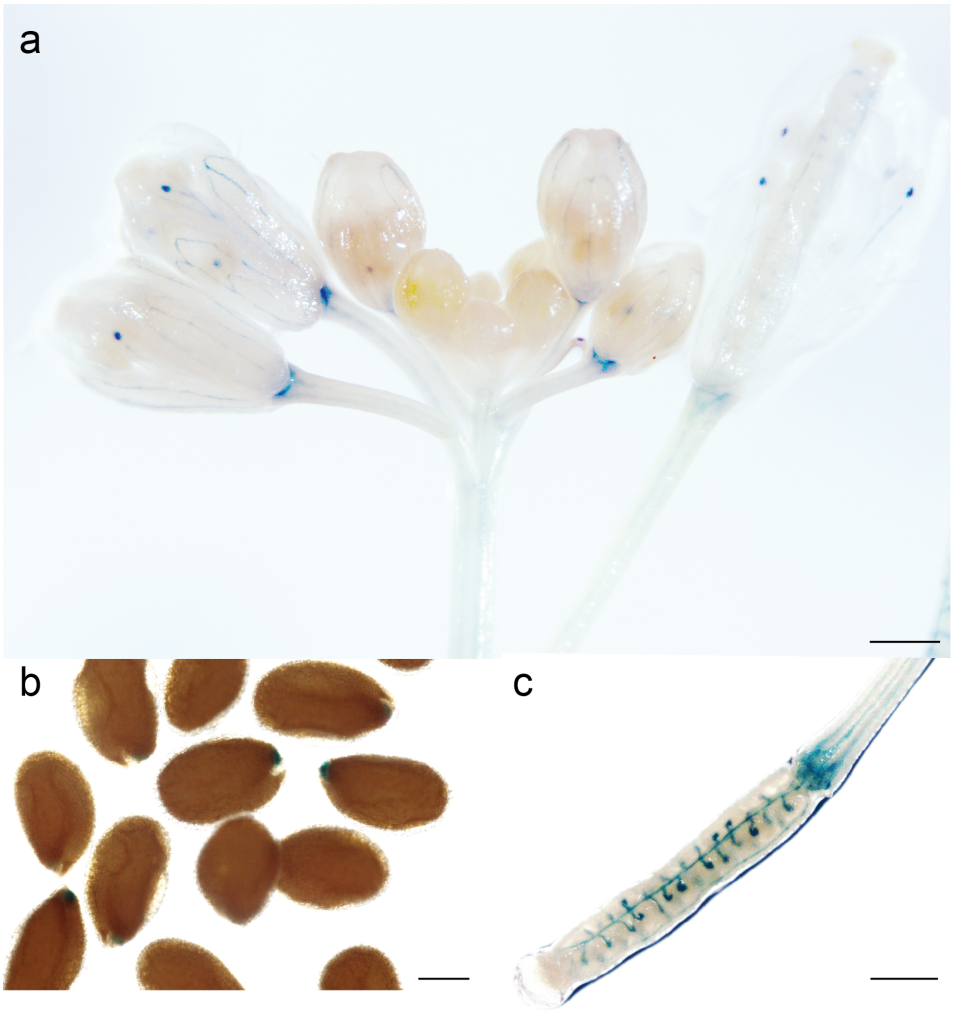

Supplementary Fig. 8: GUS staining of *pbZIP9:GFP-GUS* plants showed promoter activity in multiple tissues and organs.

a-c, GUS stained *pbZIP9:GFP-GUS* transgenic plants show GUS activity in the unloading zone of the anther, petals, and receptacle (**a**), the unloading zone of the seed coat (**b**), and the ovules, transmitting tract, and the funiculus of the ovary (**c**). Scale bars: 500 μm (**a,c**) and 200 μm (**b**).

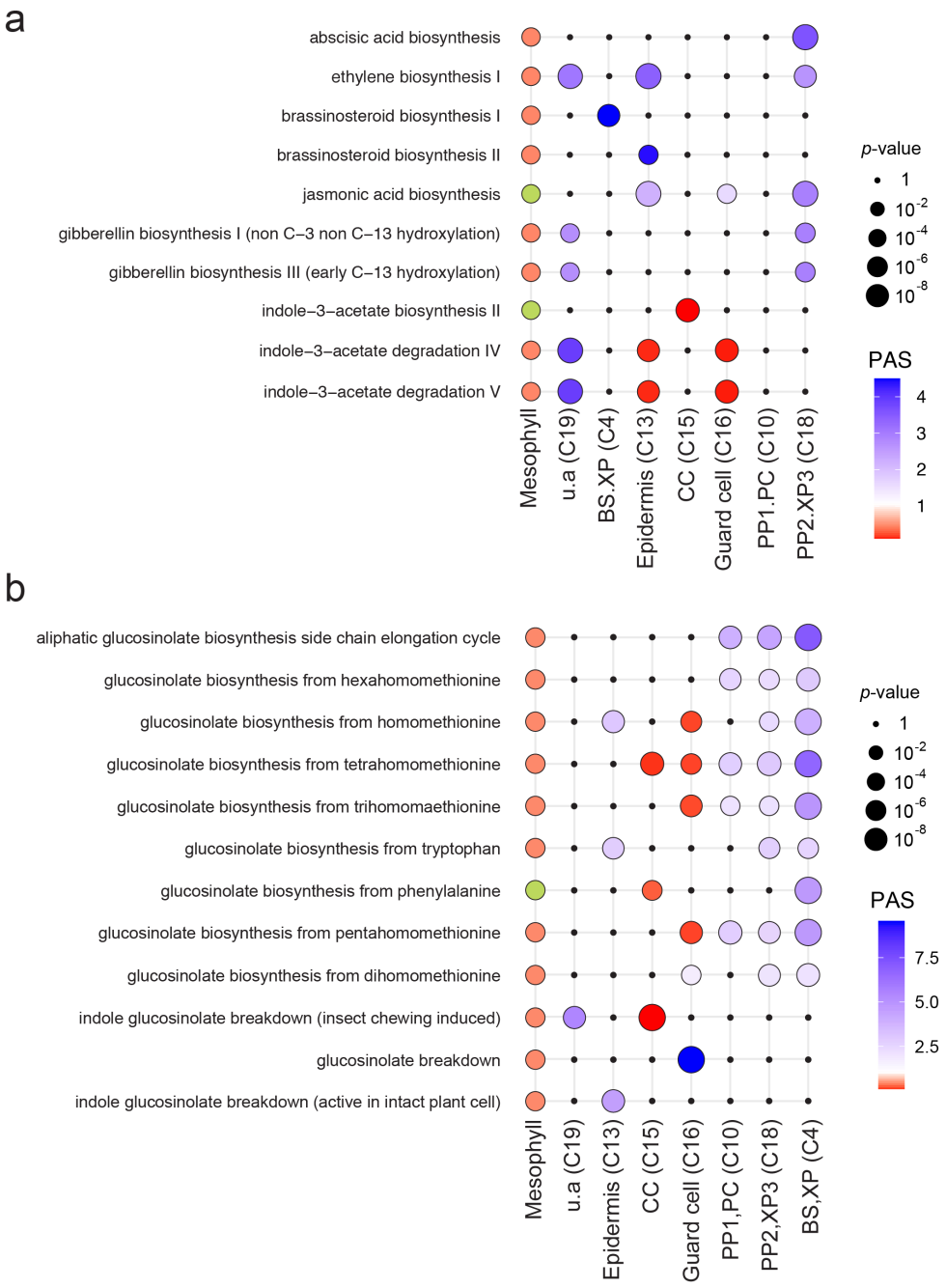

Supplementary Fig. 9: Hormone and glucosinolate pathway activity across clusters.

a, Pathway activity score (PAS) of hormone biosynthesis and degradation pathways in the indicated clusters. **b,** Metabolic pathway activities of glucosinolate biosynthesis and degradation pathways. **a,b,** The color of the dots PAS, whereas the size of the dot corresponds to its statistical significance; PASs that are statistically insignificant , *i.e.* p >0.05 in a random permutation test, are represented by black dots with 0 size. PAS<1

(red) signifies the under-representation of the genes in the pathway in the given cell type, whereas PAS > 1 (violet) signifies the over-representation of the pathway. The mesophyll cells, which form multiple clusters, are represented by a single column in both panels. Pathways represented by a red dot are significantly under-represented in at least one cluster; pathways represented by a green dot are significantly under-represented in at least one cluster, and also significantly over-represented in at least one cluster. The size of the dots in the mesophyll column does not correspond to the *p*-value of PAS.

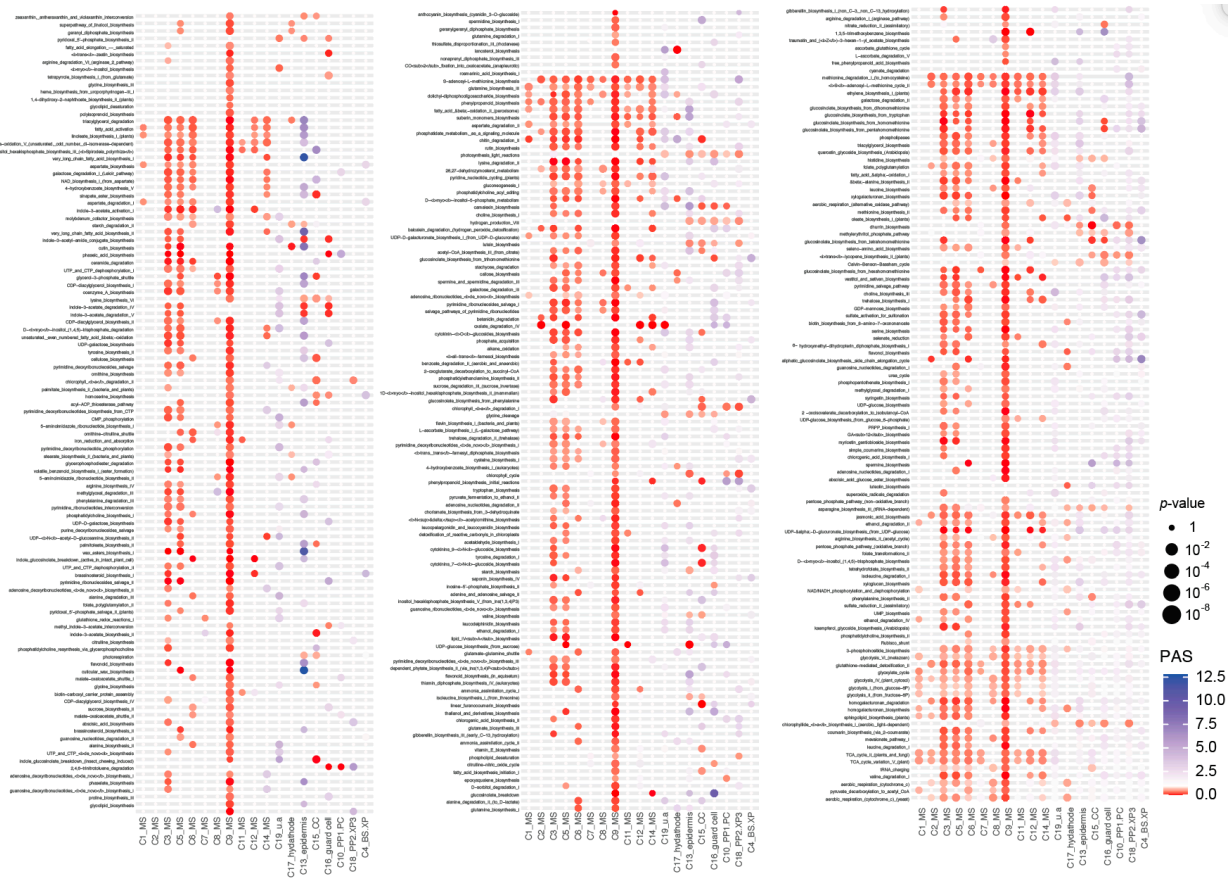

Supplementary Fig. 10: Metabolic pathway activity across all cell types. Statistical significance is represented as difference in dot size. Statistically insignificant values are left as blank (random permutation test, p >0.05). Colors represent pathway activity score (PAS); a score <1 (red) reflects a lower than average activity of the pathway in the given cell type, a score >1 (violet) indicates a higher activity.

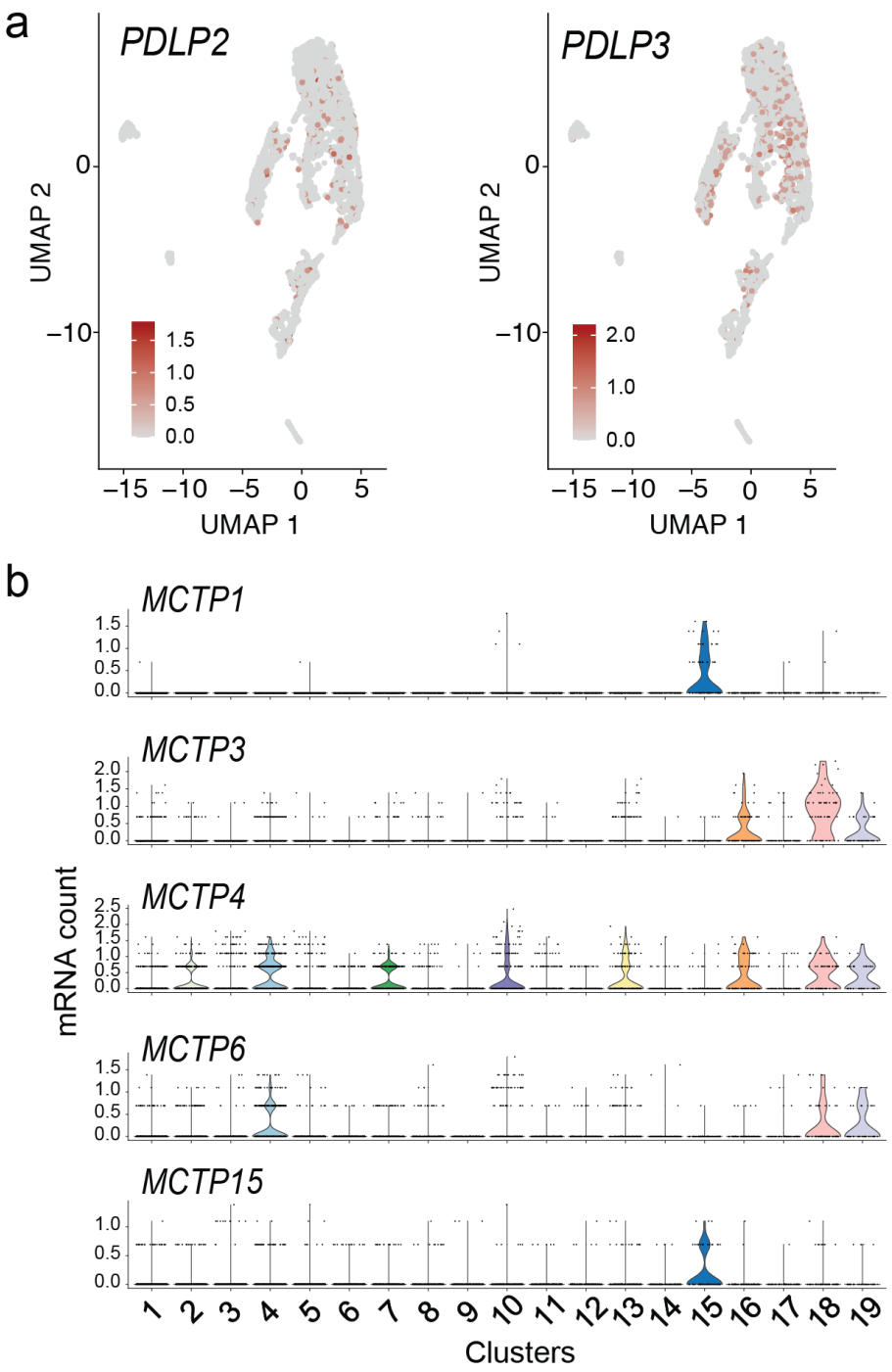

Supplementary Fig. 11: Cell type-specific transcript enrichment of plasmodesmatal proteins.

a, UMAP plot showing the distribution of *PDLP2* and *PDLP3* transcripts. **b,** Violin plot showing transcript enrichment of *MCTP*s. Note that *MCTP1* and *FTIP1* (in Fig. 3) correspond to the same gene, AT5G06850.

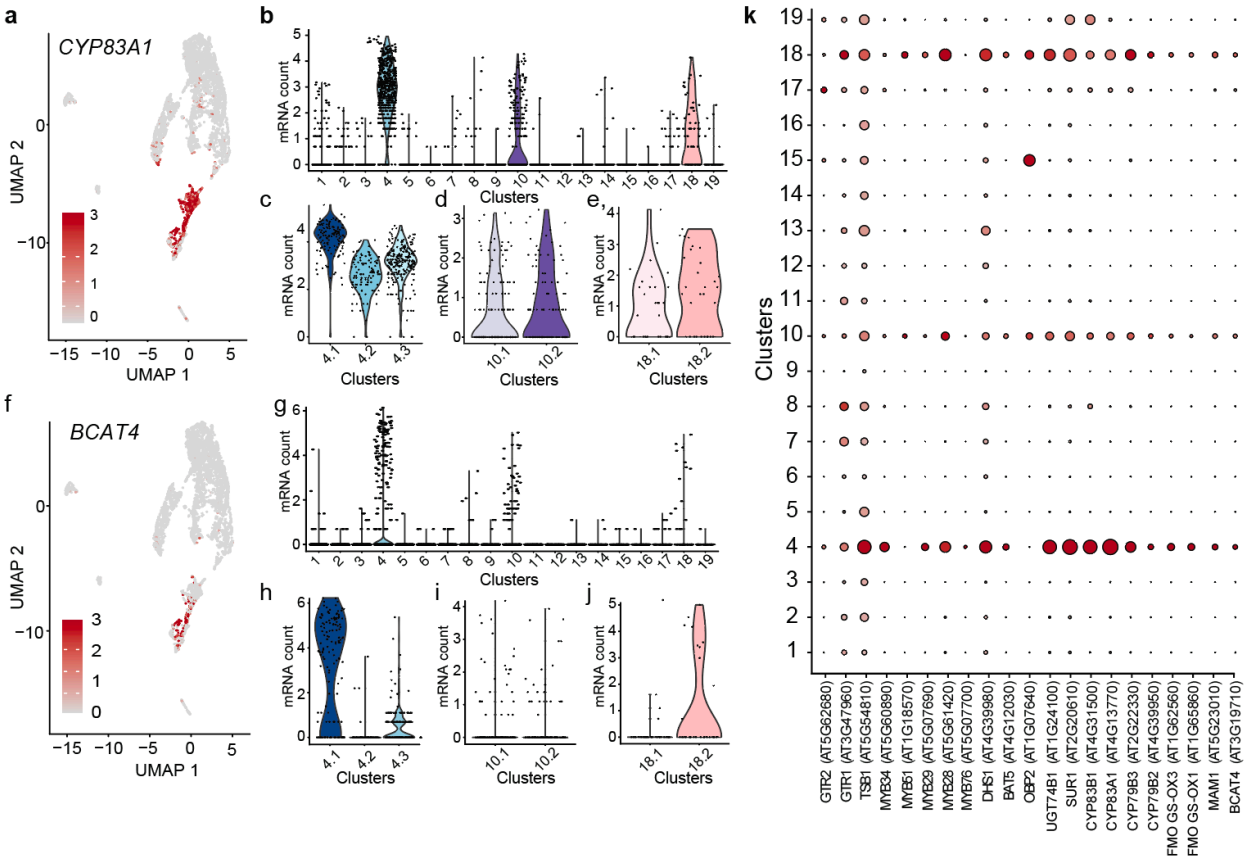

Supplementary Fig. 12: Enrichment of transcripts related to glucosinolate biosynthesis and transport

a, UMAP showing the enrichment of *CYP83A1* transcript. **b-e,** Violin plots illustrating the transcript enrichment of *CYP83A1* in BS1, BS2, XP **(b,c)**, PP1, PC^{PP}, PC^{XP} **(b,d)**, PP2 and XP3 **(b,e)**. **f,** UMAP showing the enrichment of *BCAT4* transcript. **g-j,** *BCAT4* transcript enriched in XP1, XP2 **(g,h)**, PP1, PC^{PP}, PC^{XP} **(i)**, and XP3 **(j)**. **k,** Dot plot showing enrichment of glucosinolate-related transcripts enriched in C4, C10, and C18. The diameter of the dot indicates the percentage of cells within a class, while the color encodes average enrichment across all cells within a class. These glucosinolate-related transcripts are known to be enriched in the BS, according to the translatome dataset[85].

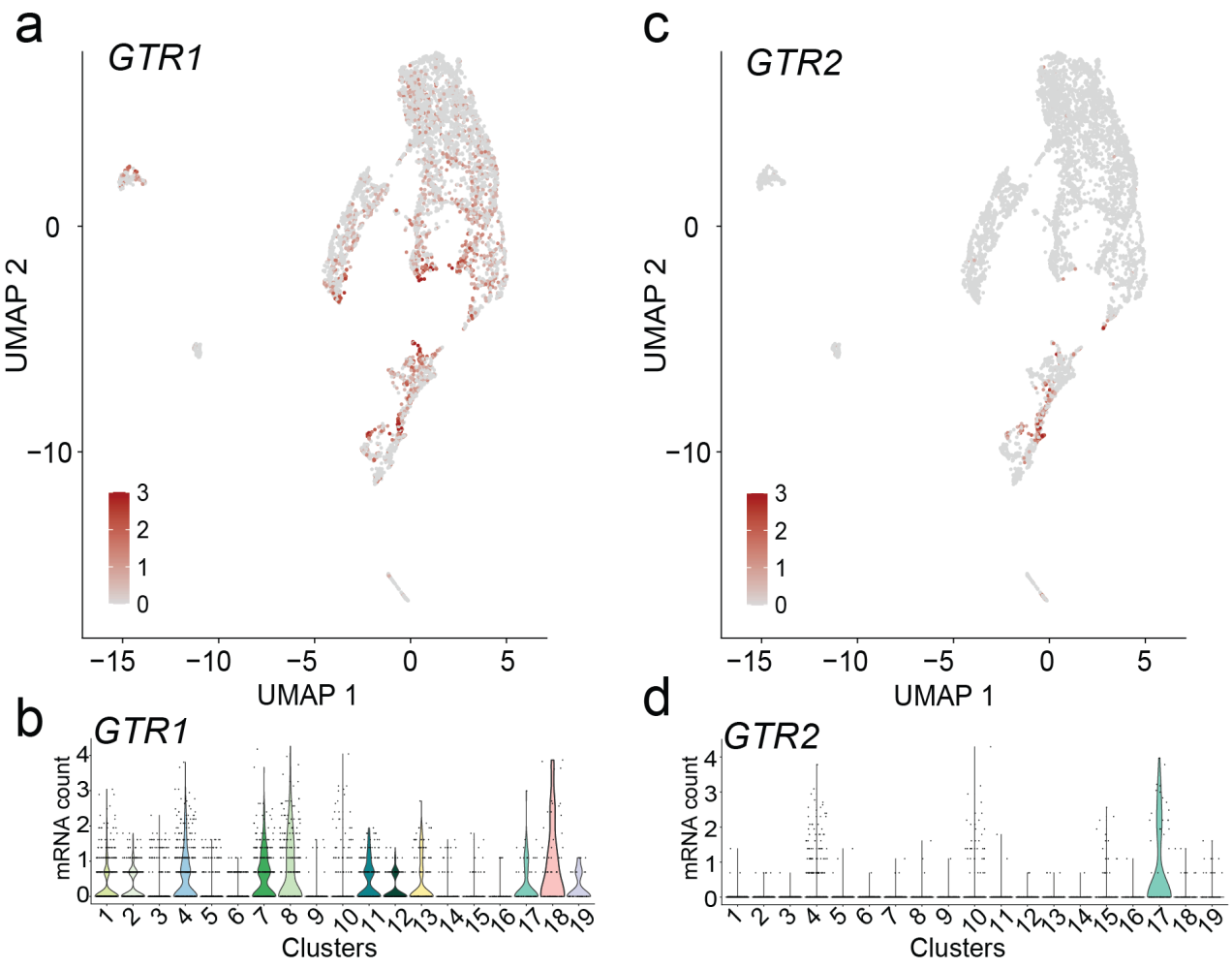

Supplementary Fig. 13: Enrichment of transcripts related to glucosinolate transport.

a,b, *GTR1* transcript detected in the broadly across C4, C7, C8, C10, C11, C12, C13, C17, C18 and C19**. c,d,** *GTR2* transcript enriched in C4, C10, and a putative hydathode cluster, C17. *GTR1* and *GTR2* transcripts were not detected in phloem related clusters (CC, PP1, PP2) (**a,c**). The broad expression pattern of *GTR1* compared to *GTR2* has been previously reported[30].

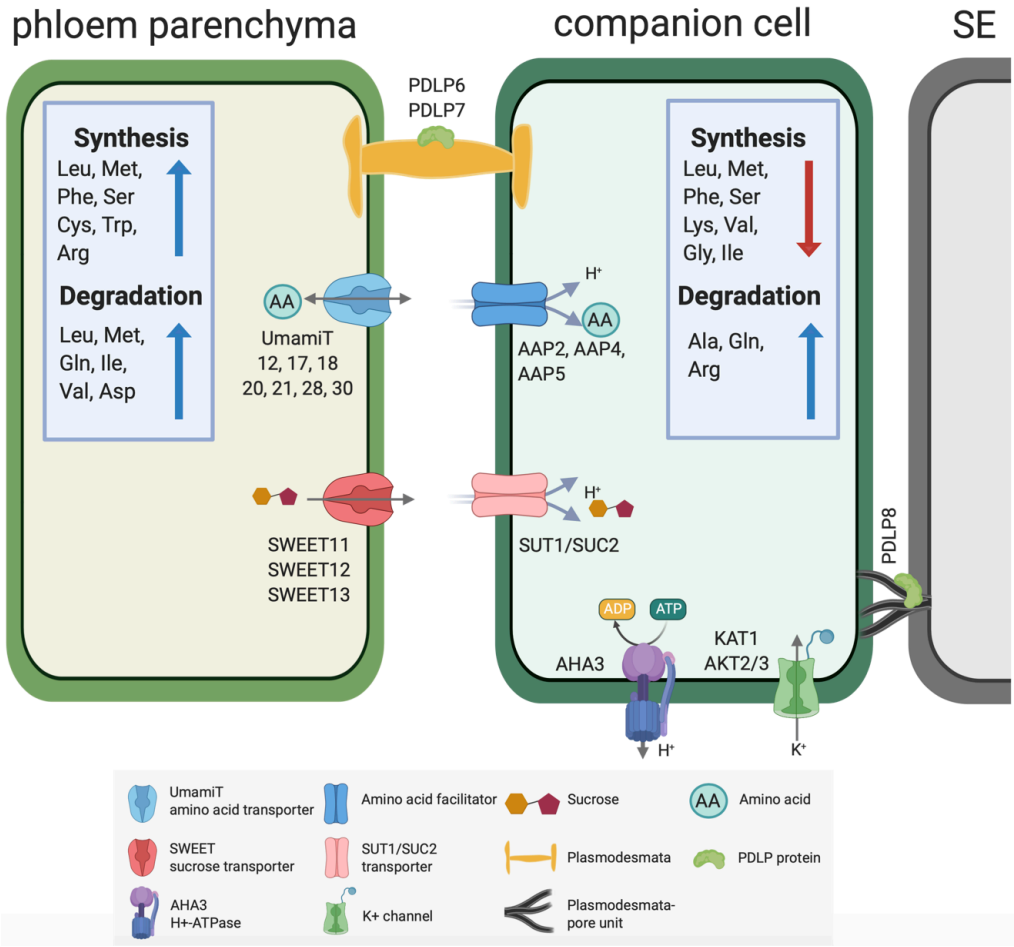

Supplementary Fig. 14: Hypothetical phloem loading process in Arabidopsis leaf.

Sucrose produced during photosynthesis in the mesophyll cells is transported across the bundle sheath to the phloem parenchyma. Biosynthesis and catabolism of multiple amino acids is highly active in the phloem parenchyma. Transporters present in the phloem parenchyma secrete sucrose (SWEET11,12,13) or amino acids (UmamiT11, 12, 17, 18, 20, 21, 28, 30) into the apoplasm. H^+/sucrose cotransporters import sucrose (SUT1/SUC2) and amino acids (AAP2,4,5) into the SE/CC. The H^+ gradient required for the active import of sucrose and amino acids into the SE/CC is provided by plasma membrane H^+-ATPases. The membrane potential is maintained by the potassium channels (KAT1 and AKT2/3). Symplasmic transport is mediated by PDLP6 and PDLP7 in the plasmodesmata in PP cells and PDLP8 enriched in the plasmodesmata-pore unit of the CC. Note that the schematic is based on transcript levels and the distribution could differ at the protein level. Schematics was made in ©BioRender – https://biorender.com